Democratic Republic of Algeria
Ministry of Higher Education and Scientific Research
University Of Kasdi Merbah Ouargla
Faculty of New Information Technologies and Communication
Department of Electronic and Telecommunication

ACADEMIC MASTER DISSERTATION

Domain : Science and Technology

Field : Electronics

Specialty : Electronics of Embedded system

Par : Mr.Mohammed Nadjib KHEMGANI

Mr.Said BOULAGUESSA

Mr.Abdellah DLILI

Thesis

MPPT Solar Using ANN, FL and P&O via Buck converter

Public discussion **30/05/2024**, before the jury composed of :

Mr.	Lati Abdelhai	MCA	in UKMO	Président
Mr.	Rouabah Boubakeur	MCA	in UKMO	Examinateur
Mr.	Bensid Khaled	MCA	in UKMO	Supervisor
Mr.	Tati Fethallah	Doctor	in UKMO	Co-Supervisor

DEDICATION

We dedicate all our gratitude and virtues to our dear parents, who helped us and spared no effort to instruct us through their sacrifice. May they find here the testimony of our deep respect and infinite recognition. To dad Ammar and Mom Yamina thank you for everything, there is nothing that can describe you from your greatness for me. To dad Mahfoud and Mom Yamina thank you for everything, there is nothing that can describe you from your greatness for me. To dad Djillali and Mom houria thank you for everything, there is nothing that can describe you from your greatness for me.
To our brothers and sisters, to those who always count on us, our moms, our aunts and uncles, our dear cousins, and our entire family. To all our friends and colleagues in this promotion. To all those who participated directly or indirectly in the realization of this work and those who hope for our success.

Remerciement

First of all, we thank God the almighty for giving us courage, patience and strength during all these years of study and that thanks to he was able to carry out this work. We would like to express our thanks and gratitude to our supervisor: Mr. Khaled bensid and Co- supervisor: Tati fethallah for the trust he has given us for the direction of this work, without ceasing to encourage us and to pushing towards the horizons of scientific research. Thanks to the Department of electronics and communications at the University And all the teachers who have taught us over the years Curriculum. thanks are also addressed to the jury members who have agreed to judge this work. Thanks to the Electrical Engineering Laboratory at the scientific research center, University of Ouargla . Finally, we also thank all our families and the people who have helped us, directly or indirectly,specially Mr.Farid Kadri in the writing of this work.

ملخص

أدت المخاوف البيئية والاقتصادية إلى تنفيذ نظام الطاقة الشمسية الكهروضوئية (النظام الكهروضوئي) لتجنب وتقليل استخدامات الوقود الأحفوري. من ناحية أخرى ، فإن الشيء السلبي هو أن كفاءة الألواح الشمسية تتدهور بسبب ارتباطها بالظروف الجوية. وبالتالي ، يجب استخدام التكنولوجيا متتبع النقطة القصوى لاستخراج أكبر قدر ممكن من الطاقة لشحن البطاريات. لا يمكن توصيل المباشر بين اللوح الشمسي و الأجهزة الإلكترونية وذلك لضياع الطاقة الكبير، ولذلك يتم توفير محول باك تيار مستمر-مستمر لشحن البطارية من المصفوفة الشمسية ، ويلعب المحول دورا مهما في تتبع نقطة الطاقة القصوى للوحة الشمسية ، بعد الانتهاء من المحاكاة ، تم تصنيع نموذج أولي واقعي للنظام المدروس باستخدام اردوينو أونو كوحدة تحكم . في هذا العمل ، تم اقتراح خوارزميات مختلفة تعتمد على منهجيات الكلاسيكية المتقدمة والاصطناعية لتوفير تحليل مقارن شامل لخوارزميات الذكاء الاصطناعي الأكثر استخداما ، وهي: الاضطراب والمراقبة ، المنطق الضبابي ، والشبكات العصبية الاصطناعية . تم استخدام بيئة ماتلاب\محاكاة لتحقيق الخوارزميات الثلاث ، وبرنامج بروتيوس وبرنامج إيسيدا لتصنيع وتركيب النموذج الأولي.

الكلمات المفتاحية: الانظمة الكهروضوئية، متتبع النقطة القصوى، محول باك(تيارمستمر-مستمر)، الاضطراب والمراقبة،المنطق الضبابي،الشبكات العصبية الاصطناعية،اردوينو اونو

Abstract

Environmental and economic concerns have led to the implementation of solar photovoltaic energy system(PV system) to avoid and reduce the uses of fossil fuels. On the other hand, the negative thing is that the efficiency of solar panels deteriorates due to its association with weather conditions. Hence, MPPT technology must be used to extract as much energy as possible to charge the batteries. The outputs obtained from a photovoltaic (PV) array cannot be connected directly to electronic devices. To regulate the output from the PV array, a DC-DC buck converter is provided to charge the battery from the solar array, and the converter plays an important role in tracking the maximum power point of the solar panel,after the completion of the simulation, a realistic prototype of the studied system was manufactured using Arduino Uno as a control unit. In this work, different algorithms based on classical and artificial AI methodologies are proposed to provide a comprehensive comparative analysis of the most commonly used MPPT AI algorithms, namely: Perturbation and Observation (P&O), Fuzzy Logic (FL), and Artificial Neural Networks (ANN). The MATLAB/Simulink environment was used to realize the three algorithms, and Proteus and easyida for the manufacture and installation of the prototype.

Keywords:PV system,MPPT,DC-DC buck converter,Perturbation & Observation,Fuzzy Logic, Artificial Neural Networks,Arduino uno.

Résumé

Les préoccupations environnementales et économiques ont conduit à la mise en œuvre de système d'énergie solaire photovoltaïque(système PV) pour éviter et réduire les utilisations de combustibles fossiles. D'autre part, le point négatif est que l'efficacité des panneaux solaires se détériore en raison de son association avec les conditions météorologiques. Par conséquent, la technologie MPPT doit être utilisée pour extraire autant d'énergie que possible pour charger les batteries. Les sorties obtenues à partir d'un réseau photovoltaïque (PV) ne peuvent pas être connectées directement à des appareils électroniques. Pour réguler la sortie du générateur photovoltaïque, un convertisseur abaisseur CC-CC est fourni pour charger la batterie à partir du générateur solaire, et la conception de l'onduleur joue un rôle important dans le suivi du point de puissance maximal du panneau solaire.simulation,un prototype réaliste du système étudié a été fabriqué en utilisant Arduino Uno comme unité de contrôle. Dans ce travail, différents algorithmes basés sur des méthodologies d'IA classiques et artificielles sont proposés pour fournir une analyse comparative complète des algorithmes d'IA MPPT les plus couramment utilisés, à savoir : Perturbation et observation (P&O), Logique floue (FL) et Réseaux de Neurones Artificiels (ANN). L'environnement MATLAB/Simulink a été utilisé pour réaliser les trois algorithmes, et Proteus et easyida pour la fabrication et l'installation du prototype.

Mots Clée : Système PV, MPPT, convertisseur abaisseur DC-DC , Perturbation & Observation, Logique floue, Réseaux de neurones artificiels, Arduino uno.

Contents

List of Figures

List of Tables

Nomenclature

Acronymes / Abréviations

ANN	Artificial Neural Networks
DC	direct current
FLC	Fuzzy Logic Controller
GPV	Photovoltaic generator
I_{ch}	Charging current (A)
I_L	Internal losses of the converter
I_m	Maximum Power point current(A)
I_{oc}	The voltage of the open circuit (V)
I_o	The saturation current of the diode
I_{ph}	The photo-current (A)
I_{pv}	Current delivered by a photovoltaic cell
I_p	Parallel resistance current (A)
I_{sc}	Short-circuit current of a solar cell or module (A)
$MPPT$	Maximum Power Point tracking
N_p	Number of modules in the panel in parallel
$P\&O$	Method of Perturbation and observation
P_L	Power of the load
P_m	Maximum power (W)

PV	Photovoltaic
R_p	Parallel shunt resistors(Ω)
Rs	Series resistance (Ω) of the cell
T	Temperature of the junction of the PV cells (K)

General Introduction

The search for alternative energy sources has become crucial due to the rising energy demand and the depletion of fossil fuel supplies. Research on renewable energy sources has been the focus of several studies aimed at identifying sustainable energy sources. Photovoltaic (PV) energy is one of the renewable energy sources that has received a lot of attention lately due to its clean, low maintenance, and noiseless nature [1]. When operating at its optimal level, the solar panel can provide the load with the highest quantity of power. The typical term for the particular operating point is maximum powerpoint (MPP).

The current-voltage characteristic of PV modules is greatly influenced by solar irradiation and cell temperature, which is why the MPP locus changes nonlinearly. Because of the nonlinearity of PV modules, the MPPT must be developed for the PV system. The PV panel MPP operating voltage may be found using MPPT at any temperature and solar irradiation level. The PV system regulates the voltage of the PV module to the MPP operating voltage. You can pull as much power as you want. The PV system's efficacy can therefore be raised [2]. in order to optimize their performance, MPPT devices need a control algorithm. The proportional–integral–derivative (PID) controller is commonly utilized in MPPT systems due to its simplicity and flexibility in implementation. However, PID demonstrates a low performance for MPPT applications with its simple structure Traditional methods such as P&O ,ANN (Artificial Neural Networks) and Fuzzy Logic [3]. in this dissertation we compared between P&O ,ANN (Artificial Neural Networks) and Fuzzy Logic. To transfer the optimum amount of electricity from the solar PV module to the load, an MPPT is utilized. Additionally, a dc-dc converter (step up/step down) transfers the greatest amount of power from the solar PV module to the load, acting as an interface between the load and the PV module [4].in this dissertation we took Buck converter as dc-dc converter

The dissertation consists of three chapters : In the first chapter, we will present a general overview of photovoltaic systems. By presenting the photovoltaic generator and the principle of photovoltaic conversion, then the modeling of the photovoltaic module.

In the second chapter, we will present the pursuit of the maximum power point, and then, the Buck converter used in our PV system. Then, we will present the three optimization methods chosen in our study (P&O, Artificial Neural Network and fuzzy logic based on MPPT).

In the last chapter, we will present the results of simulation of the comparison betwen the three algorithms and we will show the different prototype units manufactured in the laboratory in order to validate the theoretical studies presented in chapter 2.

Finally, we will end our thesis with a general conclusion that will summarize the interest of our study.

In light of the abundance of articles within this domain, a selection has been curated and presented in the following table:

Table 0.1: Previous studies

Theme	Auther	date	Method	Result
1-Fuzzy and P&O MPPT Techniques for Stabilized the Efficiency of Solar PV System	J. Kumar [5]	2018	Fuzzy P&O	eff:69% eff:65%
2-Maximum Power Point Tracking (MPPT) Scheme for Solar Photovoltaic System	Taylor and Francis [6]	2014	P&O	Tr:21%
3-Sliding mode control of a buck converter for	Amir Hussain [7]	2013	Sliding mode control	eff : 99%
4-Analysis and Comparaison of MPPT Nonlinear Controllers for PV System using Buck Converter	Taoufik Laagoubi [8]	2015	Fuzzy logic control Sliding mode control (P&O)	Tr:5.2% Tr:4% Tr:6%
5-Maximum Power Point Tracking (MPPT) Scheme for Solar Photovoltaic System	Karima Boudaraia [9]	2016	P&O	eff:98.3%
6-Comparison of Different MPPT Control Strategies	Parag K. Atri [10]	2020	(P&O) IC FOSC	eff:96.53% eff:97 % eff:93.7%
7-DC-DC Buck-Converter for MPPT of PV System	Dhananjay Choudhary [11]	2014	IC	eff:97%
8- Comparison between HC, FOCV and TG MPPT algorithms for PV solar systems using buck converter	Lahcen El mentaly [12]	2017	HC TG FOCV	eff:99% eff:99% eff:96%
9-Comparative Study on Buck and Buck-Boost DC-DC	Barnam Jyoti Saharia [13]	2016	HC	eff: 61.89%
10-The Implementation of Genetic Algorithm to MPPT Technique in a DC/DC Buck Converter under Partial Shading Condition	Prisma Megantoro [14]	2018	GA P&O	eff:98% eff:96%

Table 0.2: Previous studies

11-Intelligent Fuzzy MPPT Controller using Analysis of DC to DC Novel Buck Converter for Photovoltaic Energy System Applications	R. Arulmurugan [15]	2013	fuzzy logic Incremental conductance Perturb and observe	eff:96.51% eff:88.0% eff:85%
12- MPPT implementation and simulation using developed P&O algorithm for photovoltaic system concerning efficiency	Asaad A.H.AlZubaidi [16]	2022	p&o	eff:99.83%
13-An investigation on maximum power extraction algorithms from PV systems with corresponding DC-DC converters	Khaled Osmani [17]	2021	p&o IC HT	eff:98.7% eff:96% eff:99.6%
14- Design and Implementation of Low Cost MPPT Solar Charge Controller	Shamrat Bahadur [18]	2022	proportional integral (PI) control loop	eff:90%
15-Experimental implementation of a novel scheduling algorithm for adaptive and modified P&O MPPT controller using fuzzy logic for WECS	Hicham Gouabi [19]	2021	P&O	eff: 99.47%
16-IMPLEMENTATION OF PERTURB AND OBSERVE MPPT OF PV SYSTEM WITH DIRECT CONTROL METHOD USING BUCK AND BUCK-BOOST CONVERTERS	Ahmed M Atallah [20]	2014	p&o	eff: 93.79%
17-An efficient Fuzzy Logic MPPT Control Approach for Solar PV System: A Comparative Analysis with the Conventional Perturb and Observe Technique	Mounir Dabboussi [21]	2020	FLC p&o	Tr:6% Tr:8%

Table 0.3: Previous studies

18-Réalisation d'un chargeur de Batterie Basé sur La commande MPPT photovoltaïque	DRAIDI, Djazira [22]	2022	FLC p&o	eff:93%
19-MPPT command and control of a system photovoltaic 3KW by fuzzy logic	HAKOUMI Ahmed,BENAMAR Abdeldjalil [23]	2019	p&o	eff:97.53%
20-New approach to adaptive MPPT used in the Photovoltaic System	ABDELLI, Fatiha,BAALI,Souad [24]	2023	p&o ADC INC	Tr:15% Tr:5% Tr:15%
21-Enhancing Solar Smartphone Charger Efficiency Through MPPT Technology	Muhammad Hilman Hakimi Yunus [25]	2024	Incremental Conductance (INC)	Eff:95%
22-ANFIS-based improved GWO: Rapid prototyping of low-power solar energy system under fast-changing solar radiation conditions	Goksel Gokkus [26]	2024	Grey Wolf (GWO)	Eff:97.22%
23-Comparative Analysis of Improved Efficient Converter Topologies with Mppt Techniques for Battery Charging Using Photovoltaic Arrays in Electric Vehicle Applications	Linda Johnsana [27]	2024	Hybrid PSO and P&O MPPT Controller	Eff:94.3%
24-An Innovate on hybrid power generation on DC–DC Buck converter with MPPT systems	Nivedita Kshatri [28]	2020	P&O INC. CON	eff:80.6% eff:82.83%

After reading all these researches and articles we found that the effect ranges from 61.89%,88%,98.7% and 99.6% as the best result of the Article N. 9, N. 11, N. 13(Twice) and of the table in order.
and about the time of response ranges from 21%,15%,8%and 4% as the best result of the Article N. 2, N. 20, N. 17 and N. 4 of the table in order.
And we are going to improve this results .

Chapter 1

General information about photovoltaic systems

1.1 Introduction

Renewable energy sources have become an increasingly significant part of the global energy consumption mix due to rising concerns about the environmental effects of greenhouse gas emissions from fossil fuels, high and unstable energy prices, and the geopolitical environment surrounding fossil fuel production [29]. These energy sources are limitless , free and highly environmentally friendly. One of the greatest possibilities is solar energy because it is a clean, renewable energy source that is widely available. The earth receives from the sun enough energy every ninety minutes to cover the planet's annual energy needs. Even though solar energy is so plentiful, it still makes up a very small portion of the world's energy supply today. But this is quickly changing as a result of international efforts to reduce climate change and enhance energy access and supply security [30].

This chapter serves as a succinct review of solar generators (fields, modules, and cells). Next, we demonstrate PV module modeling and electrical parameter identification. A simulation of a 59.4 W photovoltaic module concludes our discussion.

1.2 Photovoltaic generator :

Solar photovoltaic energy is produced by directly converting a portion of the sun's radiation into electrical energy. Utilizing a cell known as a photovoltaic cell, which is based on the physical phenomena known as the photovoltaic effect—the generation of an electromotive force when this cell's surface is exposed to light—this energy conversion is accomplished [31]. The power generated by a basic solar cell pales in comparison to what is required for the majority of industrial or home applications. An elementary cell a few tens of square centimeters in size can generate a few watts maximum at a voltage of less than one volt [32].

1.2.1 Solar radiation :

Solar radiation consists of photons whose wavelength extends from ultraviolet to infrared. To characterize the solar spectrum in terms of emitted energy, the notion AM is used for "Air Mass". In space outside the Earth's atmosphere (AM0), the energy transported by solar radiation over a sun-earth distance is of the order of (1350 W/m^2)(Figure 1.1). Passing through the atmosphere, the solar radiation undergoes a decrease and a modification of its spectrum due to the phenomena of absorption and diffusion in gases. Its value is of the order of (1000 W/m^2) at ground level, at 90° of inclination (AM1) [33,34].

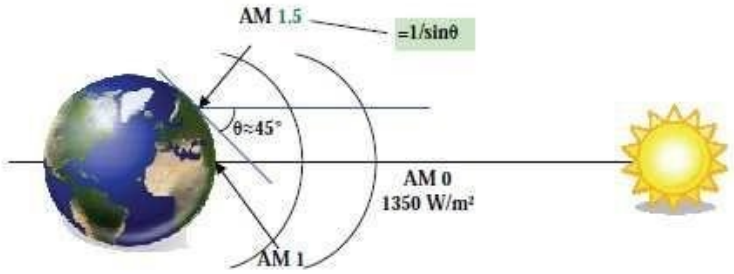

Figure 1.1: Normes de mesures du spectre d'énergie lumineuse émis par le soleil, notion de la convention AM

The value of the global radiation received on the ground is determined by adding to the latter the diffuse radiation which concerns the radiation whose trajectory between the sun and the observation point is not geometrically rectilinear and which is scattered or reflected by the atmosphere or the ground. Considering this, we obtain a reference of the global spectrum rated AM1.5 with a power of (1000 W/m^2), (Figure 1.2) corresponding to our latitudes [33, 35].

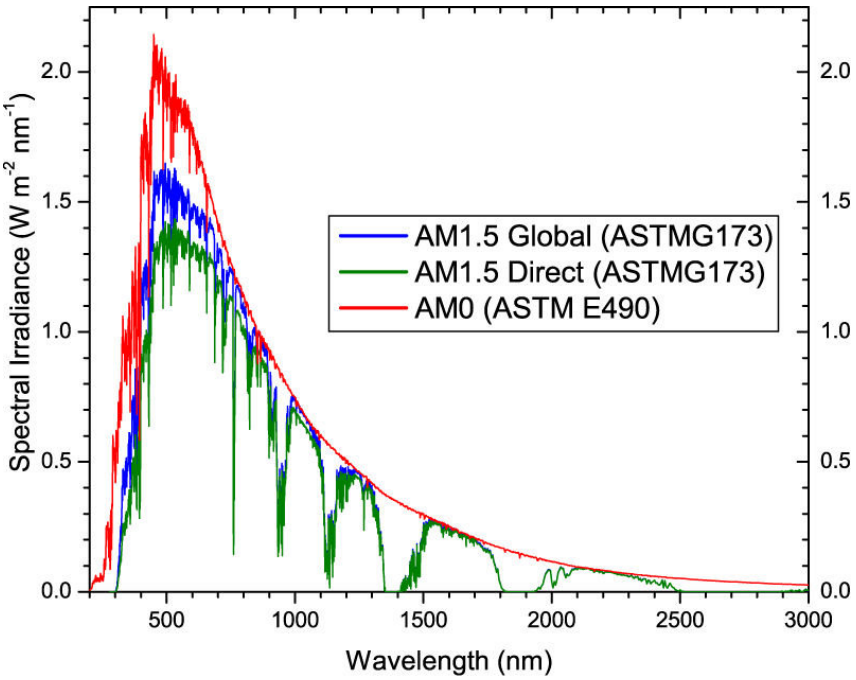

Figure 1.2: Spectres Solaires relevés dans plusieurs conditions selon la convention AM

.

1.2.2 Photovoltaic module :

To produce more power, the solar cells are assembled to form a module. The series connections of several cells increase the voltage for the same current, while paralleling increases the current while maintaining the voltage. These cells are protected from moisture by encapsulation in an EVA (ethylenevynil-acetate) polymer (see Figure 1.3) and protected on the front surface of a high-temperature tempered glass transmission and good mechanical strength and on the back surface of polyethylene [36].

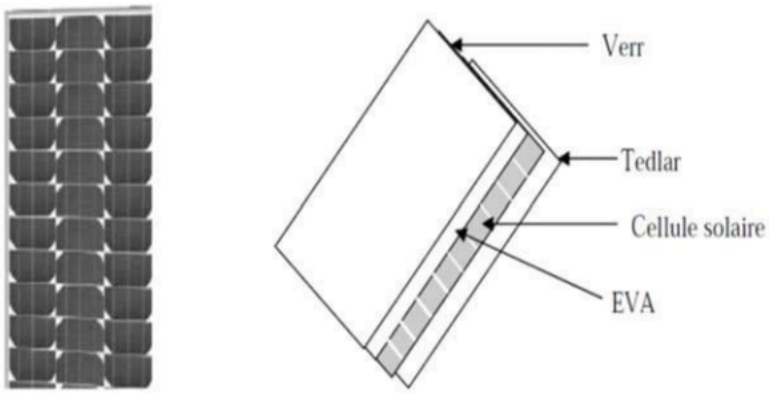

Figure 1.3: Photovoltaic module

.

1.2.3 Photovoltaic field :

photovoltaic field is the association in series and in parallel of several panels photovoltaics. In the serial association, the panels are crossed by the same current while that the voltages of each panel add up. This is the complete opposite of the signs photovoltaic cells connected in parallel; they are subjected to the same voltage while the currents of each of the panels are added to give the total current of the field. The series-parallel association therefore makes it possible to achieve the desired currents and voltages in order to to supply high-power loads [37, 38].

Figure 1.4: Photovoltaic field

1.3 Generator of Photovoltaic cells :

Over the last ten years, photovoltaics have emerged as a significant player in the continuing energy revolution. Developments in materials science and production techniques have played a major part in that evolution. Still, a lot more work needs to be done before photovoltaics can produce cheaper, greener energy. Research in this area focuses on printable solar cell materials like quantum dots, graphene or intermediate band gap cells, and efficient photovoltaic devices like multi-junction cells [39].

1.3.1 Photovoltaic cell:

A photovoltaic cell is an optoelectronic component that transforms directly solar light into electricity, was discovered by E. Becquerel in 1839. One-cell photovoltaic is constituted by a semiconductor material of the P-N type. The size of each cell is a few square centimeters [40].(Figure 1.5) represents a schematic sample of a configuration of the photovoltaic cell [41].

.

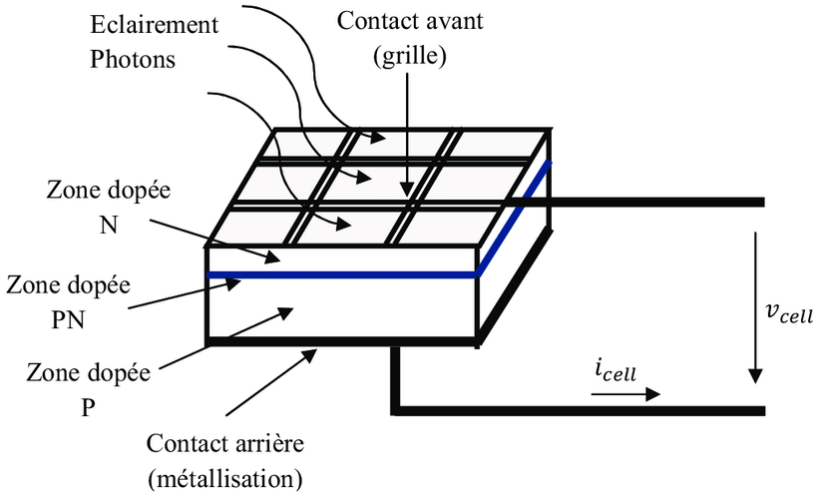

Figure 1.5: Photovoltaic cell

1.3.2 Development of efficiency in Photovoltaic cells :

Efficiency potential of high-efficiency solar cells such as crystalline Si,GaAs, GaAs/Si, CIGSe, and CdTe solar cells has been discussed based on ERE, Voc loss, and FF loss. Detail results will be presented elsewhere. (Figure 1.6) shows summary for potential efficiencies of various high- efficiency solar cells. In summary, crystalline Si solar cells have potential efficiency of 28.8% with normalized series resistance and shunt resistance rs + 1/rsh of 0.05 by improvements in ERE from around 1% to 30%. GaAs have potential efficiency of 30.0% with rs + 1/rsh of 0.025 by improvements in ERE from 22.5% to 40%. III-V 3-junction and 5-junction cells have potential efficiencies of 40% and 43% with rs + 1/rsh of 0.05 by improvements in ERE from 0.05% to 1% and from 0.005% to 1%, respectively. CuInGa(S,Se)2 and CdTe cells have potential efficiencies of 26.5% and 26.4% with rs + 1/rsh of 0.05 by improvements in ERE from around 0.5% to 10% and from around 0.1% to 5%, respectively. Perovskite cells have potential efficiency of 24.9% by improvements in ERE from around 0.1% to 5%. For this end, further improvements in minority-carrier lifetime based on understanding defect behavior in addition to improvements in front surface, rear surface, and interface passivation and decease in series resistance and increase in shunt resistance are suggested to realize higher efficiency solar cells [42].

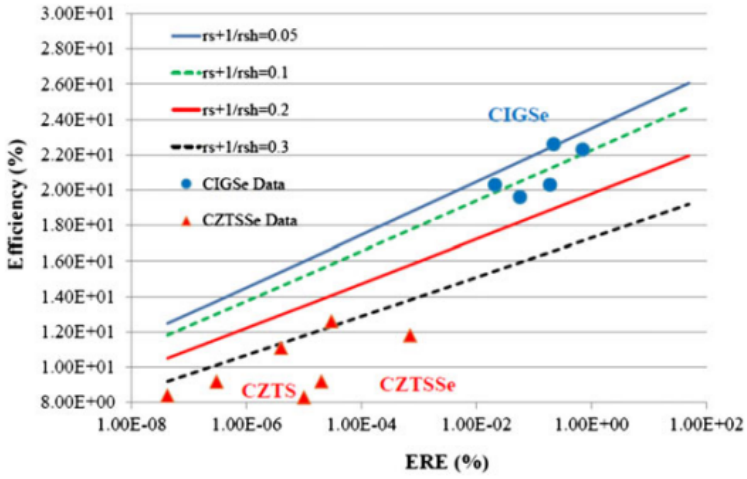

Figure 1.6: Efficiency potential of various high-efficiency solar cells

1.3.3 Types of Photovoltaic cells :

1.3.3.1 The Monocrystalline cells

A cell that forms when a block of silicon crystallizes into a single crystal is referred to as a monocrystalline cell. has a uniform color and a round shape that can occasionally be virtually square. Panels with monocrystalline cells provide a yield of 14–18%. Their production process is still costly and intricate [36].

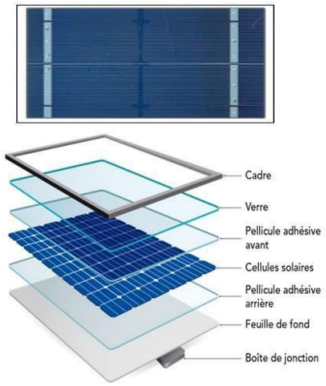

Figure 1.7: Monocrystalline

1.3.3.2 The polycrystalline cells :

A silicon block that crystallized into many crystals is the source of the polycrystalline cells. They frequently take the form of a rectangle. Although the cost of producing solar panels using polycrystalline cells is lower, their yield ranges from 11-15% [36].

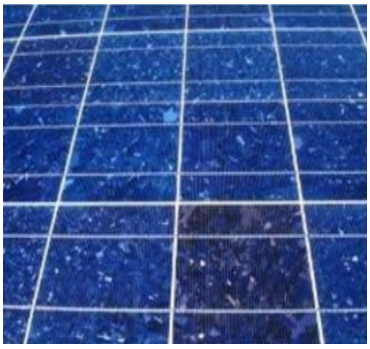

Figure 1.8: polycrystalline

1.3.3.3 The Amorphous cells :

A "silicon gas" is projected onto glass, flexible plastic, or metal by a vacuum vaporization process to create amorphous photovoltaic cells. It is possible to use extremely thin silicon layers thanks to this method. Compared to earlier models, these solar cells have a yield of 7-9% and a lower production cost [36].

Figure 1.9: Amorphous

1.4 Modeling of the photovoltaic module :

To comprehend a photovoltaic system's output characteristics, performance evaluation, and behavior analysis under temperature and radiation variations, modeling and simulation are essential [43].

1.4.1 Case of an ideal cell :

In the ideal case, the cell of a PN junction subjected to photovoltaic illumination connected to a load can be schematized by an I_{ph} photodiode current generator in parallel with a diode delivering a current I_d. (Figure 1.10)illustrates the electrical circuit equivalent to the ideal solar cell [44].

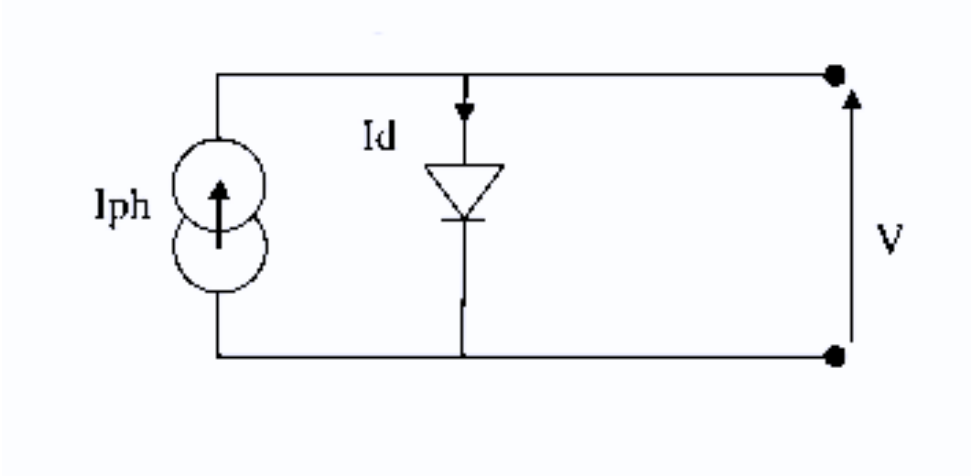

Figure 1.10: Electrical circuit equivalent to the one-diode model

1.4.1.1 The current of panel solar I_{pv}

The equations retained from this model are:

$$I_{pv} = I_{ph} - I_d \tag{1.1}$$

1.4.1.2 Photo-current I_{ph}

The Iph current is assimilated to the short-circuit current obtained in the short cycle of the I_{sc} load where $V_{pv} = 0$ [44].

$$I_{ph} = I_{sc} = \frac{Ir}{Ir_{ref}} \tag{1.2}$$

with:
Ir: The illuminance absorbed by the cell.
Ir_{ref}: Reference illuminance (1000 W/m^2).

1.4.1.3 Diode Current I_d:

$$I_d = I_s(e^{\frac{vd}{vt}} - 1) \tag{1.3}$$

With:
I_s: Diode Reverse Saturation Current [A].
V_d: Voltage of diode[V].

1.4.1.4 Thermal voltage V_t:

$$V_t = \frac{NKT}{q} \tag{1.4}$$

With:
N: Ideality factor of the solar cell.
K: Boltzmann's constant($1.3805.10^{-23}$ J/K).
q: Charge of the electron($1.6.10^{-19}$ C).

1.4.2 Case of a real cell :

The performance of a solar cell (Figure 1.11), is limited by the influence of two physical phenomena comparable to two resistances R_s and R_{sh} [44].

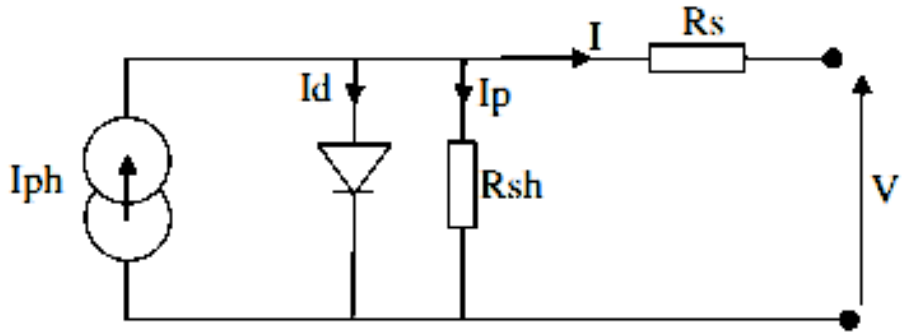

Figure 1.11: Equivalent electrical circuit of a real cell

1.4.2.1 Series resistance R_s:

due essentially to losses by Joule effects through the grids of collections and the own resistance of semiconductors, as well as to bad contacts (semiconductors, electrodes) [44].

$$R_s = \frac{V_{pm}}{I_{pm}} - \frac{BN_cV_tR_p}{I_0R_pexp(\frac{V_{pm}+I_{pm}R_s}{BN_sV_t}) + BN_cV_t} \tag{1.5}$$

1.4.2.2 Shunt resistance R_{sh}:

Parallel resistance, called "Shunt", comes from losses by recombination due essentially to the thickness, to the surface effects, as well as to the non-ideality of the PN junction [44].

$$R_{sh} = \frac{V_{pm} + I_{pm}R_s}{I_{ph} - I_{pm} - I_0[exp(\frac{V_{pm}+I_{pm}R_s}{BN_cV_t}) - 1]} \tag{1.6}$$

1.4.2.3 Identification of GPV parameters:

The current-voltage characteristic equation of the GPV which stems from the solar cell is

$$I_{pv} = I_{ph} - I_0[e(\frac{V_{pv} + I_{pv}.R_s}{V_t}) - 1] - \frac{V_{pv} + I_{pv}.R_s}{R_p} \tag{1.7}$$

$$I_{pv} = I_{ph} - I_s(exp(\frac{q(V + R_sI)}{AKT}) - 1) - \frac{V + R_sI}{R_{sh}} \tag{1.8}$$

With:
I_{pv}: Current of PV.
K: Boltzmann's constant($1.3805.10^{-23}$ J/K).
q:Charge of the electron($1.6.10^{-19}$ C).
K: Boltzmann's constant($1.3805.10^{-23}$ J/K).

1.4.2.4 The Ideality Factor A:

The ideal factor of the diode depending on its technology (material) is included usually between 1 and 2.

1.4.2.5 the saturation current Is:

the reverse saturation current of the diode, the saturation current Is varies with temperature according to the following equation:

$$I_s = \frac{I_{sc} + a_v(T - T_{ref})}{exp(\frac{V_{oc} + a_v(T - T_{ref})}{AKT}) - 1} \tag{1.9}$$

With:
V_{oc}: the open-circuit voltage of the cell (V).
a_v: the temperature coefficient of the open-circuit voltage (V/K).

1.4.2.6 Photo-current I_{ph}:

the photon current of the diode (A) The (I_{ph} I_{sc}) hypothesis is typically used in the modeling of PV modules because in practical modules, the series resistance is low and the parallel resistance is high. [44] The photon current generated by the PV cell from light linearly depends on illuminance and is also influenced by temperature. A better approximation can be made by using the resistors in series and in parallel to calculate the current, as shown in this Equation :

$$I_{ph} = \frac{(R_s + R_{sh})I_{sc}}{R_{sh}} \tag{1.10}$$

The I_{ph} current varies with temperature according to the equation below:

$$I_{ph} = \frac{Ir}{Ir_{ref}}(I_{sc} + a_i(T - T_{ref})) \tag{1.11}$$

With:

Ir: The illuminance absorbed by the cell (W).

Ir_{ref}: Reference illuminance (1000 W/m^2).

I_{sc}: Standard short-circuit current (under standard conditions).

T_{ref}: reference temperature (298.15 K).

a_i: the temperature coefficient of the short-circuit current (A/K).

1.5 Identification of PV module parameters :

It is common knowledge that the first step in determining any system's parameters is a crucial stage for practice as well as simulation. Therefore, for simulation, quality control, and performance estimations, exact information on the photovoltaic modules' properties is necessary, just like for any other system. PV cell and panel manufacturers typically supply a data sheet (datasheet) with some specifications of the PV panel, which comprises several cell groups. However, the spec sheet does not provide all of the characteristics. finding these unknown characteristics is crucial in real-world applications, We conducted our research on a 60 W solar panel to determine the parameters of the PV panel.

Table 1.1: Features of 59.4 W PV Panel

Maximum power	P_{max}	59.4	W
Current at maximum power	I_{Pm}	3.3	A
Maximum Point Voltage	V_{Pm}	18	V
Open-Circuit Voltage	V_{oc}	22.2	V
Short-circuit current	I_{sc}	3.56	A
Diode saturation current	I_s	$5.8049.10^{-11}$	A
Diode Ideality Factor.	A	1.9347	/
Shunt resistance	R_{sh}	210.3819	Ω
Series resistance	R_s	0.46344	Ω

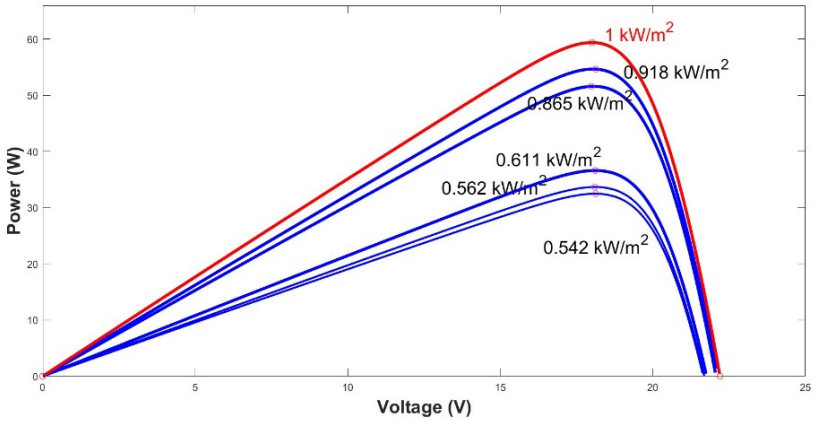

Figure 1.12: Power-Voltage Characteristics

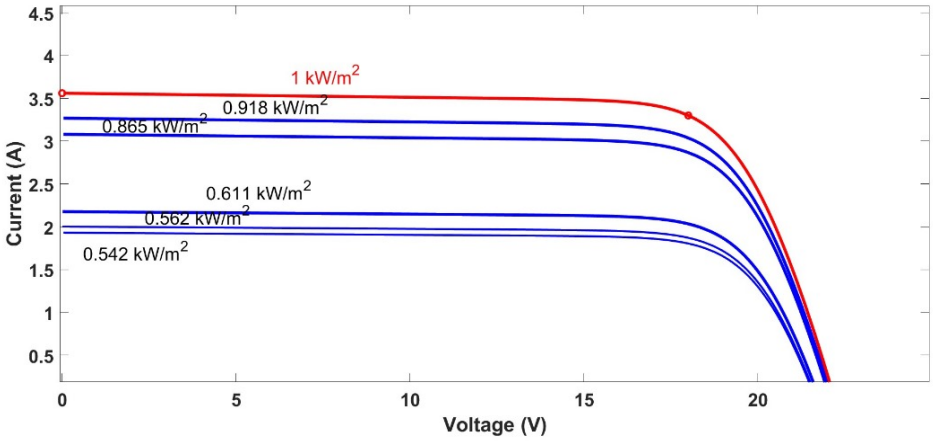

Figure 1.13: Current-voltage characteristic

1.5.1 Iterative method :

The iterative technique is a strategy to determine the parameters of the solar panel with error minimization because all parameters depend on each other [45]. It is advised to use the Newton-Raphson approach to solve equations (12),(13) and (14) to iterate the parameters and minimize the error indicated in equation (15).

$$E_{rr1} = \frac{V_{mpp}}{I_{mpp}} - \frac{BN_cV_tR_p}{I_0R_pexp[(\frac{V_{mpp}+I_{mpp}R_s}{BN_cV_t})] + BN_cV_t} - R_s \tag{1.12}$$

$$E_{rr2} = \frac{V_{mpp} + I_{mpp}R_s}{I_{ph} - I_{mpp} - I_0[exp(\frac{V_{mpp}+I_{mpp}R_s}{BN_cV_t}) - 1]} - R_p \tag{1.13}$$

$$E_{rr3} = \frac{R_p + R_s}{R_p}I_{cc} - I_{ph} \tag{1.14}$$

$$E_{rr} = (E_{rr1})^2 + (E_{rr2})^2 + (E_{rr3})^2 \tag{1.15}$$

1.6 Conclusion :

This chapter is devoted to the presentation of the photovoltaic generator. We have studied the photoelectric generator of various generated forces (cells, modules, fields). Next, the modules need to be modeled and the electrical parameters need to be determined, the effects of temperature, illumination, and series and parallel resistors (RS and Rs, respectively) in addition to the current and voltage. We will examine DC-DC converters (Buck), and their MPPT commands in the upcoming chapter in order to locate the solar generator's maximum powerpoint.

Chapter 2

The maximum power point tracking

2.1 Introduction

As we saw in the last chapter, temperature and solar illumination affect a photovoltaic generator's performance. The maximum power point fluctuates as a result of these climate variables. To extract and transfer the maximum possible power at the terminals of the photovoltaic generator to the load at all times, we need an adaptation stage that plays a role in transferring the maximum power supplied from the generator The adapter commonly used in PV is a static converter (power converter DC/DC). The conversion structure is chosen according to the load to be supplied. In this chapter, we will study the direct connection between the photovoltaic generator and the load. The DC-DC converter used in our photovoltaic system is of buck type, So, we describe the MPPT control of the DC-DC converters by the algorithms perturbation and observation (P&O) and Fuzzy Logic and Artificial Neural Network [40].

2.2 Direct connection between the photovoltaic generator and load

There is no mechanism inserted in between the GPV and the load when they are directly coupled [46].

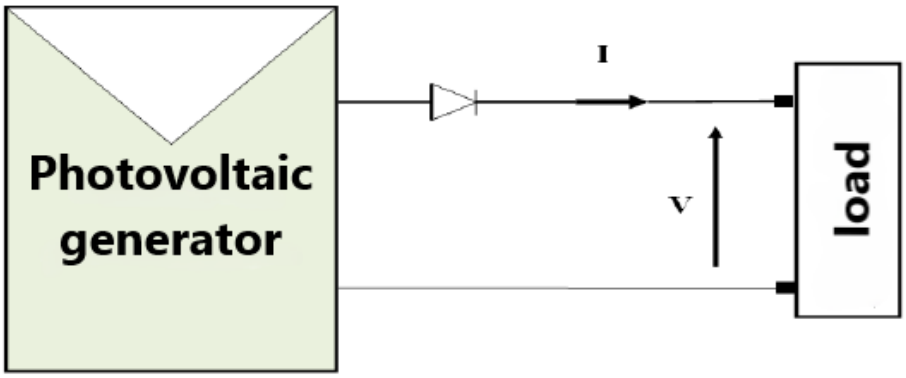

Figure 2.1: Direct GPV-load coupling

The figure (2.2) represents a practical test of the direct coupling of a resistive load of R= 100 , to a photovoltaic generator of 10.29 w, according to these results, it is found that the power supplied by the GPV is equal to 4.08 W. (Pch = 20.4x0.2 = 4.08 w) [40].

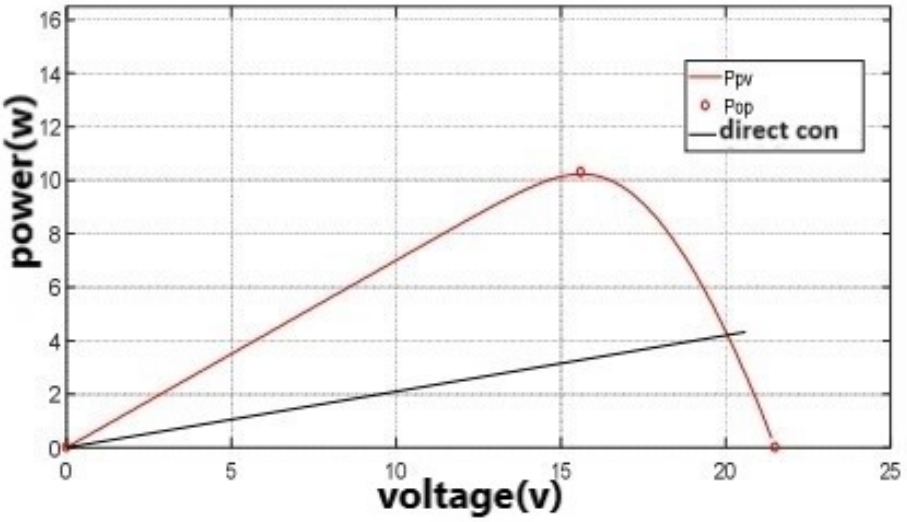

Figure 2.2: Practical test of direct coupling GPV-resistive load (R=100)

The features of the load that the PV generator is linked to have a significant impact on how well it operates. Furthermore, the best adaptation happens at a single maximum power point, or maximum point power, MPP, for various values of Resistors. As a result, the most widely used method to ensure that the generator runs at its peak efficiency is to add a DC/DC converter, which functions as a source-load adaptor and allows the generator to produce its maximum power in this scenario.

2.3 Power converter

Continuous input current DC-DC converters are widely utilized in systems to optimize solar energy, wind energy, fuel cells, and batteries. Additionally, dc-to-dc converters—also known as active front-end converters—are the fundamental building blocks for AC input, unity power factor single and three-phase ac-to-dc converters [47]. In order to meet our needs, the voltage provided by the photovoltaic panels is of the DC kind. A variety of DC-DC converters, or choppers, are available.

2.3.1 DC/DC Converter

New technology electronic devices must meet certain criteria such as high quality, reliability, size, weight, and reduced cost [48]. Linear power regulators, the principle of operation of which is based on a current or voltage divider, can provide a very high-quality output voltage [48, 49]. However, this type of regulator remains ineffective due to the fact that their main field of application is at low power levels [50]. Switching regulators called DC / DC converters use electronic switches, based on semiconductors such as the thyristor, power transistor, or IGBT ... etc, because they generate a low power loss when switching from one state to another [51]. These converters ensure high energy conversion efficiencies and they can operate at high frequencies. The dynamic characteristics of DC/DC converters improve with increasing operating frequencies. The high operating frequencies therefore make it possible to achieve a faster dynamic response to rapid changes in the charging current or the input voltage [50].

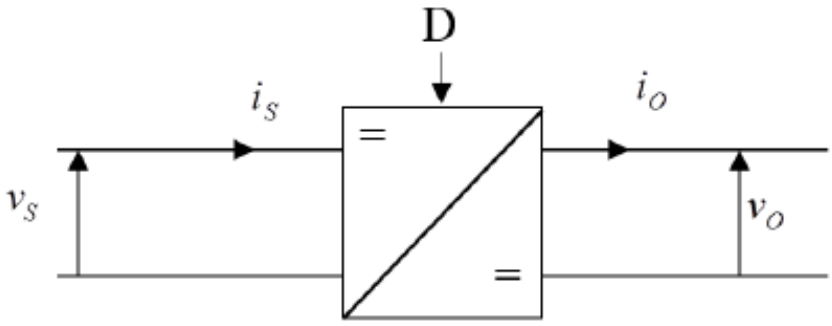

Figure 2.3: Symbol of a DC/DC chopper

2.3.2 Buck converter

A buck converter is a type of converter that lowers voltage and is used to connect solar arrays to resistance loads (RL) through the use of a battery. Consisting of electronic switches, diodes, inductors, and capacitors, the buck converter circuit [52], which are shown in figure 2.4.

$$Vo = Vi * D \tag{2.1}$$

$$Vo = \frac{Vi}{1 - D} \tag{2.2}$$

$$L = \frac{Vo(1 - D)}{\Delta i_L . f} \tag{2.3}$$

$$C = \frac{1 - D_i}{8L(\frac{\Delta Vo}{Vo})(f^2)} \tag{2.4}$$

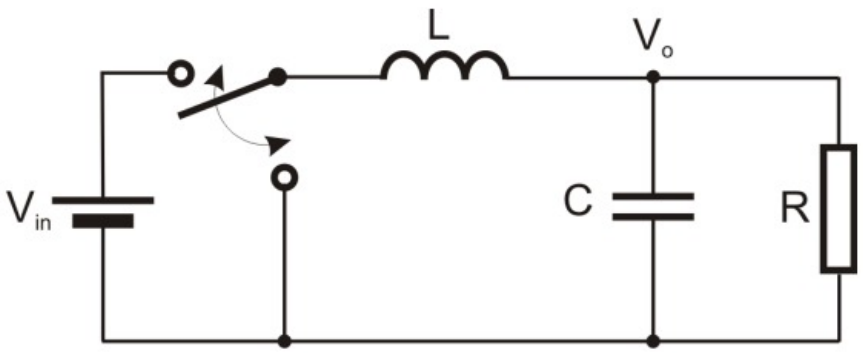

Figure 2.4: DC-DC converter

A buck converter is an electronic device that helps to regulate voltage by lowering a DC supply's voltage while increasing its current. There are two ways to activate the switch state. When the switch is first closed or turned on, the inductor produces an opposing voltage in response to a change in current. This results in a decrease in voltage across the load. When the switch is turned off or opened again, the voltage source is eliminated from the circuit, and as a result, the current drops. The inductor's magnetic field helps to facilitate current passage through the load, and a change in current will lead to a change in voltage across the inductor. The motor now releases its stored energy into the circuit [52, 53].

2.3.2.1 ON state of the switch

The switch is ON during the time t satisfying the relation $(0 < t < t_{ON})$. During this interval of time, the equivalent the scheme is illustrated in Figure 2.5

The equivalent ON circuit-related equations are depicted as following:

$$\frac{diL(t)}{dt} = \frac{1}{L}(V_{in} - Vo) \tag{2.5}$$

$$\frac{dVo(t)}{dt} = \frac{1}{C}(i_{in} - \frac{Vo}{R}) \tag{2.6}$$

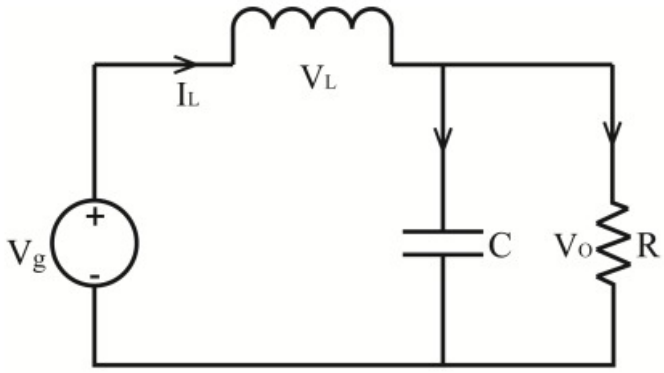

Figure 2.5: DC converter equivalent scheme during ON switch state

2.3.2.2 Off state of the switch

The switch is Off during the time t satisfy the relation ($t_{ON} < t < t_{OFF}$). During this interval of time [54], the equivalent scheme is illustrated in Figure 2.6 The equivalent OFF

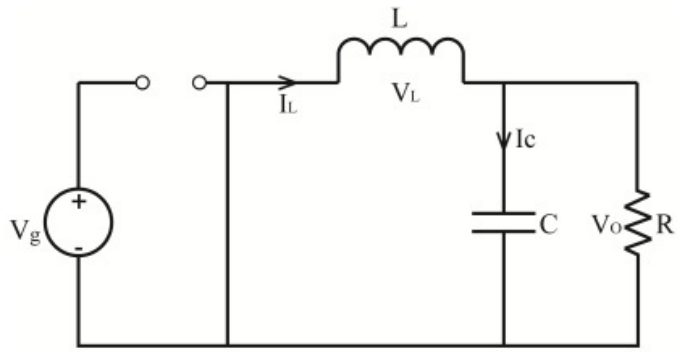

Figure 2.6: DC converter equivalent scheme during Off switch state

circuit-related equations are depicted as following:

$$\frac{di_L}{dt} = \frac{1}{L}(-Vo) \tag{2.7}$$

$$\frac{dVo}{dt} = \frac{dV_c}{dt} = \frac{1}{c} \times i_c = \frac{1}{C}(i_L - \frac{Vo}{R}) \tag{2.8}$$

$$\frac{I_0}{I_D} = \frac{1}{D} \tag{2.9}$$

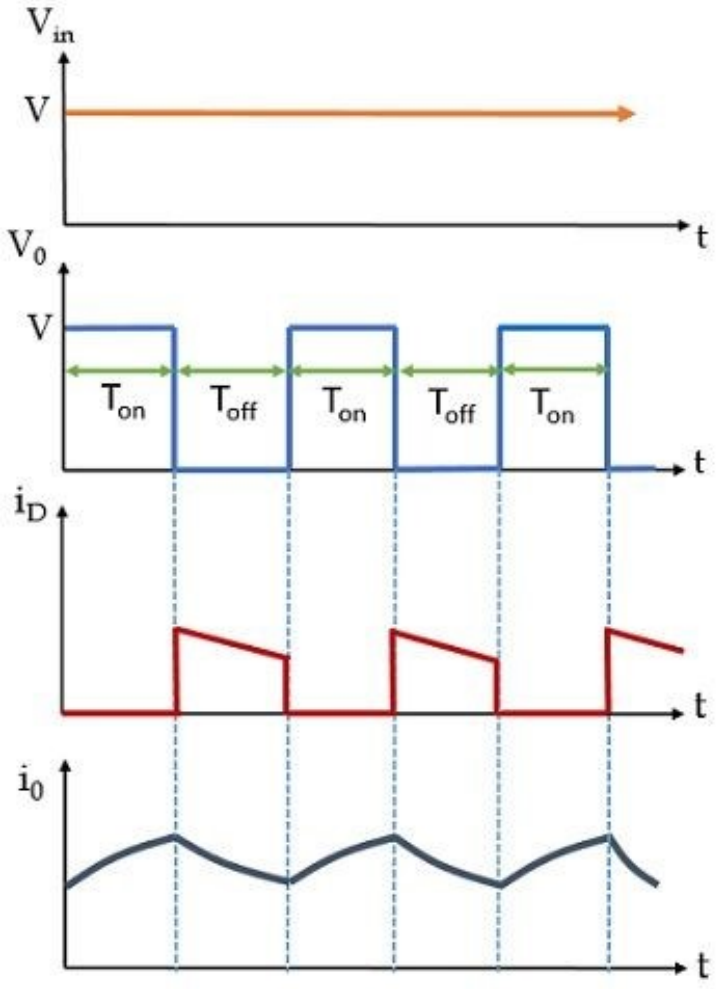

Figure 2.7: Waveform of the input and output voltages and currents of the "Buck"

2.4 Tracking of the maximum power point

Maximizing the PV generator's power is necessary to increase the system's performance. This is achievable if the operating point is properly selected by adjusting the charge's impedance to the source. The DC-DC converter will function as an impedance adaptor, ensuring optimal operation and enabling the PV generator to produce its maximum power [55].

Thus, to optimize the power of a photovoltaic source, it is necessary to search for this optimal operating point. The follower of the maximum power point is called this command. These MPPT techniques are based on iterative research methods to determine the optimal operating point of the solar module, to reach the maximum power without disturbing the operation of the system. They are based on the constant optimization of the power produced by photovoltaic solar panels.

It is possible to calculate the extracted power using the current and voltage measure-

ments of the module, and then multiplying these two quantities. Different algorithms use these measurements to track the actual MPP. Different types of MPPT algorithms are available, such as the perturbation and observation algorithm and the fuzzy logic-based MPPT algorithm.

2.4.1 Perturbation and observation algorithm (P&O)

Due to its straightforward design and ease of application, the perturb and observe algorithm is thought to be the most widely used MPPT algorithm among the other methods. It is predicated on the idea that, as shown in Figure 2.8 [56], at the top of the power-voltage curve, the change in the PV array output power is equal to zero ($\Delta P_{PV}= 0$). The PV array $P(n+1)$ output power is compared to the output power at the preceding perturbation $P(n)$ using a periodic perturbation (increment or decrease) of the PV array terminal voltage or current. A perturbation in terminal voltage should be maintained in the same direction if it increases PV power ($\Delta P_{PV}> 0$); otherwise, it should be moved in the other way. The cycle of perturbation is iterated until the maximum power is reached at ($\Delta P_{PV}= 0$). P&O's control flow chart is displayed in Figure 2.9. The P&O method can be implemented in two different ways. Since a reference voltage is typically utilized as a perturbation parameter, a PI controller is needed to adjust the duty ratio [56]. The second way is that the duty ratio is directly perturbed and the power is measured every PWM cycle This technique's benefits are its simplicity, ease of application, and lack of need for prior understanding of the PV array. But, the P&O will continue to swing around the MPP, causing some needless power loss, even after it is reached. [56]

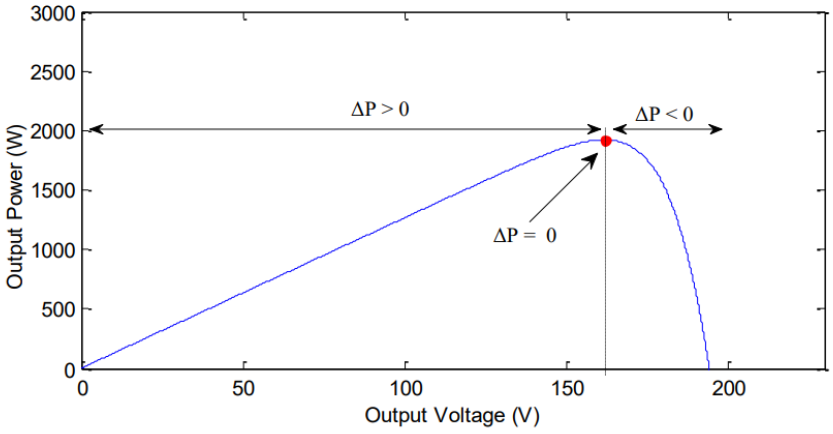

Figure 2.8: Sign of the dP/dV at different positions on the power characteristic

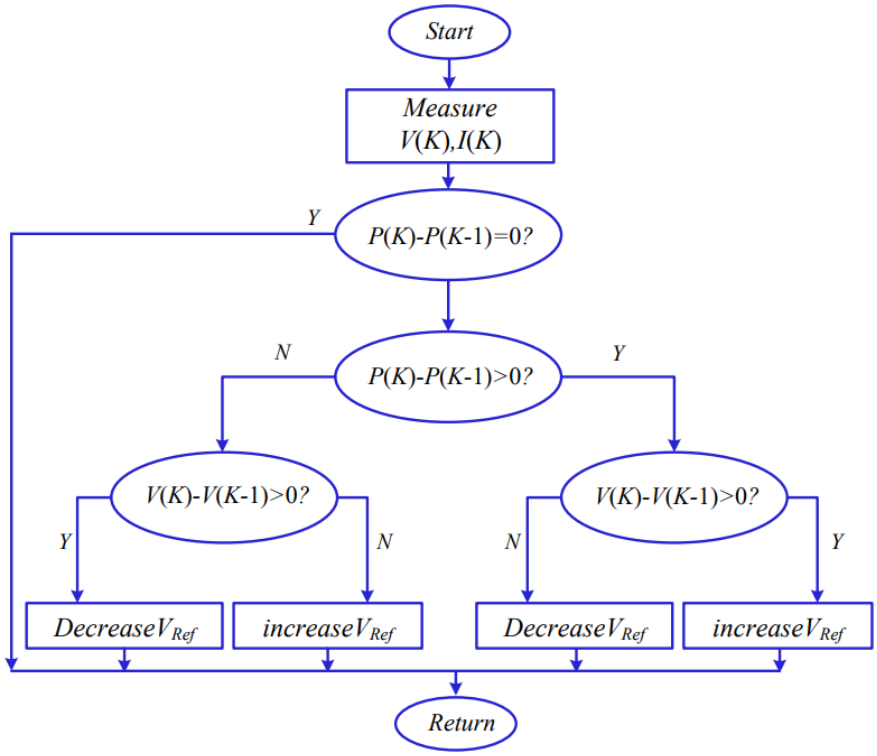

Figure 2.9: Flowchart of the P&O algorithm

2.4.2 Artificial Neural Network

Artificial neural networks (ANNs) are adaptive systems designed to mimic how the human brain works. These are systems with the capacity to alter their internal

structure to a functional goal. Because they can recreate the fuzzy rules governing the best solution for nonlinear issues, they are especially well-suited to solving these problems. The connections and nodes, commonly referred to as processing elements (PE), are the fundamental components of an artificial neural network. Every node has an input from which it receives messages from other nodes, the environment, or both, and an output from which it can communicate with the environment or different nodes. Lastly, every node contains a function f that it uses to change its global input [57]. Its components are:

2.4.2.1 Input Layers

The initial layer of an ANN is called the input layer, and it is here that different texts, numbers, audio files, picture pixels, and other types of input data are fed into the system [58].

2.4.2.2 Hidden Layers

The hidden layers are located in the center of the ANN model. As in the case of a perceptron, there can be one hidden layer,or there might be several hidden layers.

Each neuron in a hidden layer receives inputs from the neurons in the previous layer, performs a computation using weighted sums of these inputs, applies an activation function to the result, and then passes the output to the neurons in the next layer. This process is repeated for each neuron in the hidden layer, allowing the network to learn complex patterns and relationships within the data , [58].

2.4.2.3 Bias

Bias is the simplifying assumptions made by a model to make the target function easier to learn [58, 59].

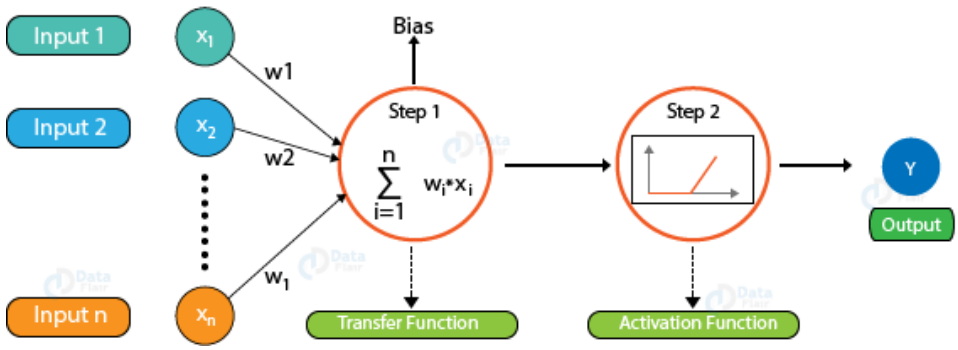

Figure 2.10: proposed design of the artificial neural network (ANN).

2.4.2.4 Activation Function

By computing the weighted sum and then applying bias, the activation function determines if a neuron needs to be stimulated or not. Adding non-linearity to a neuron's output is the aim of the activation function. We are aware that each neuron in the neural network responds to weight, bias, and its corresponding activation function. Based on the mistake in the output, we would adjust the weights and biases of the neurons in a neural network. We call this method back-propagation. Back-propagation is made possible by activation functions, which provide the gradients and error together for updating the weights and biases [60, 61].

Function	Formula
Log sigmoidal	$f(x) = \frac{1}{1+e^{-x}}$
Tan sigmoidal	$f(x) = \frac{1-e^{-x}}{1+e^{-x}}$
Hyperbolic tangent	$f(x) = \tanh(x)$
Pure linear	$f(x) = x$
Inverse tangent	$f(x) = \frac{2}{\pi}\tan^{-1}(x)$
Gaussian radial basis	$f(x) = \exp\left(-\frac{\|x-m\|^2}{\sigma^2}\right)$
Linear	$f(x) = ax + b$
Threshold	$f(x) = \begin{cases} 1, & x>0 \\ -1 & x<0 \end{cases}$

Figure 2.11: Various activation functions used in artificial neural network modeling.

2.4.2.5 Principle of the ANN algorithm

Each input is multiplied by a corresponding weight(w1,w2, ... w,), analogous to synaptic strength. All the weighted inputs are summed up to determine the activation level of neuron, NET. Where:

$NET = x_1w_1+x_2w_2+...+x_nw_n$ The activation function f(X) further processes the NET signal to generate the output signal (y_i) of the neuron, during the computation within a neuron, the bias is added to the weighted sum of the inputs before passing through the activation function. This allows the neuron to have a certain level of activation even when all the inputs are zero, effectively controlling the threshold at which the neuron becomes active [62].

$$y_i = f(\sum_{i=1}^{n} x_i w_i - \theta) \tag{2.10}$$

Where w_i: is the connection weight. θ:is the bias. x_i: is the inputs. y_i:is the output.

2.4.2.6 ANN-based MPPT algorithm

ANN approach is applied on a huge real training dataset to find a PV array's highest power point [63]. The simulation of the MPPT algorithm based on ANN for a PV system is considered using irradiation as input and the duty cycle as output

2.4.2.7 Principle of training ANN-based MPPT algorithm

Firstly we have to run a simulation model PV array to get the data (input) and the target in our case we use P&O algorithm after that we start training the ANN if we reach the required performance, it means the ANN is trained otherwise we have to train it again until we get the required performance [64].

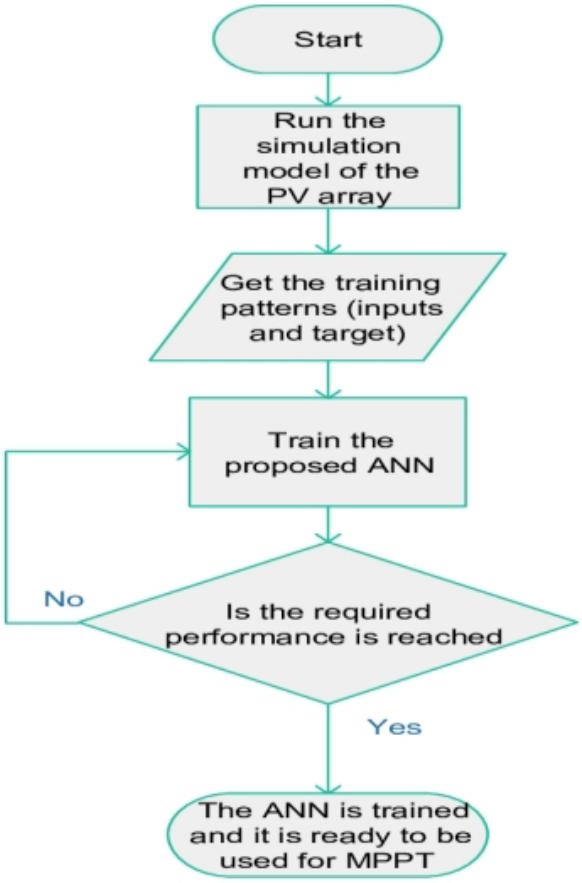

Figure 2.12: A flowchart of the training process of the ANN for MPPT.

2.4.3 Fuzzy Logic

In 1965 (Zadeh 1965), Professor L. A. Zadeh of the University of California, Berkeley, introduced fuzzy logic in his article "Fuzzy sets". [65]Two types contain fuzzy regulator "SUGENO" and "MAMDANI" ,and we used Mamdani.
Fuzzy logic is a new approach based on artificial intelligence as well as is a well-known soft computing tool that Develops applicable algorithms by including structured human knowledge. It is a logical system that provides A model designed for human interpretation patterns that are Inaccurate and not accurate. A fuzzy logic system can be Applied to the design of intelligent systems based on information expressed in human language. The approach is derived from the decomposition of a set of variance of a real variable in the form of linguistic variables and the assignment of an organic function to each variable. The rules developed on the basis of the experience of a human operator are expressed in a linguistic form. Define the rules Dynamic performance of Fuzzy Logic Controller Fuzzy logic deals with problems that Inaccuracy , ambiguity, approximation , uncertainty Or qualitative chaos or partial truth [65, 66].

The proposed fuzzy logic controller includes four basic elements: fuzzification unit, rules of base, inference engine and defuzzification [67].

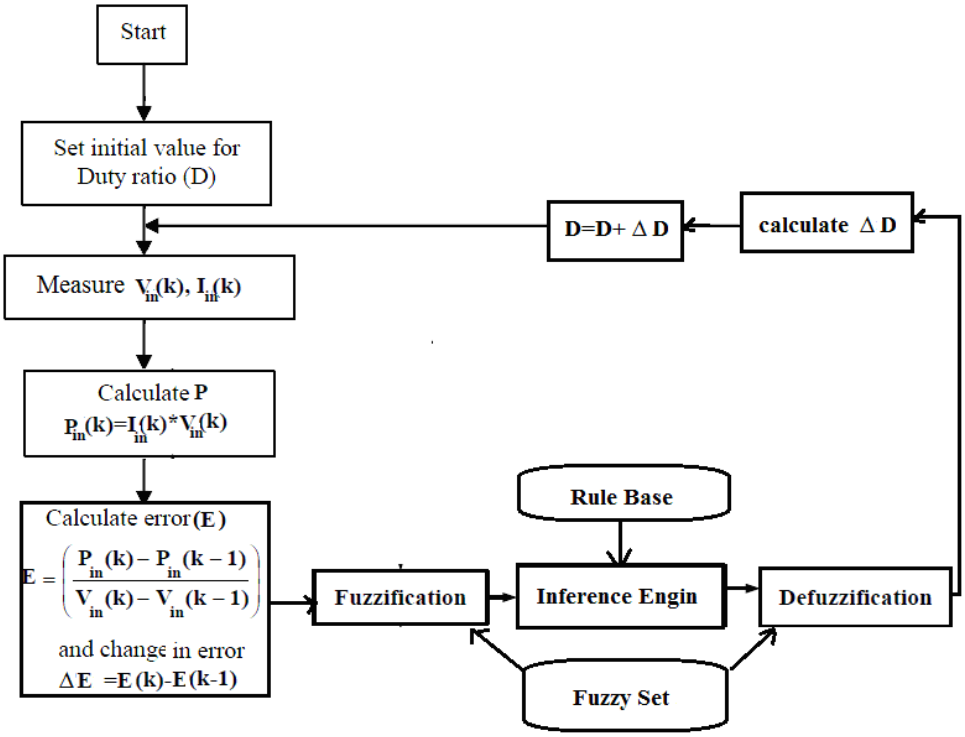

Figure 2.13: Flow chart of Fuzzy logic MPPT

2.4.3.1 fuzzification

The fuzzification unit deals with the conversion of real variables to fuzzy variables. E(k) and CE(k) are fuzzy logic controller inputs given by the equations(2 .11, 2.12). E(k) represents the derivative of P_{PV}(k). E(k) is canceled when the operating point reaches the MPPT. CE(k) is the error of E(k). Voltage and current are measured for power calculation P_{PV}. The output of the fuzzy logic controller d_D is the variable step of the duty cycle [66].

$$E(k) = \frac{I(k) - I(k-1)}{V(k) - V(k-1)} + \frac{I(k)}{V(k)} \tag{2.11}$$

$$CE(k) = E(k) - E(k-1) \tag{2.12}$$

Figure 2.14 shows the selected membership functions of E, CE and d_D. Among the different forms of membership functions (trapezoid, Gaussian and triangular...), the symmetrical triangular shape is considered the most appropriate for its simplicity. The boundaries of the fuzzy variable range are usually normalized between -1 and + 1 by introducing a gain factor to represent the real signals . In this study, the symmetrical triangular shape has been selected and the limits are considered as ([-0.04, 0.04] and [-100, 100] and [-0.04, 0.04]) for (E, CE and d_D) respectively [66].

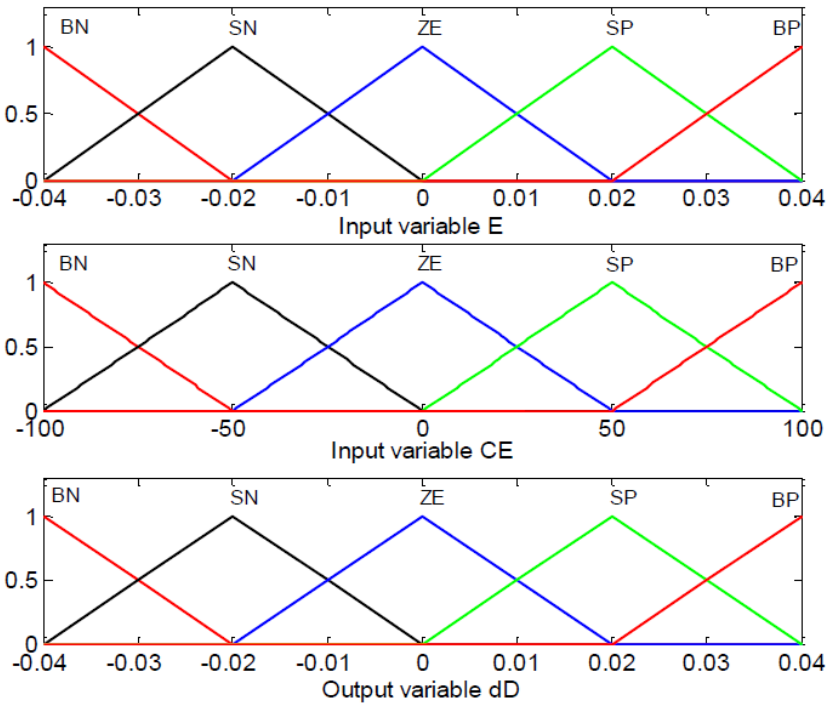

Figure 2.14: Membership functions of the input (E, CE) and output (d_D) variables.

2.4.3.2 inference engine and rules of base

The fuzzy interface strategy that is most frequently employed is the Mamdani method. Ever since it was first proposed in 1975 by University of London professor Ebrahim Mamdani, who constructed one of the enigmatic systems for operating a steam engine and boiler together.
The Mamdani technique used a series of imprecise rules that were supplied by knowledgeable human operators.Fuzzy extensional logic describes process states using linguistic variables, which are then used as inputs to govern grammar. Linguistic variables are vague combinations of a particular type of phrase. Although different forms are feasible, trapezoidal or triangular fuzzy arrays are typically used in Mamdani fuzzy logic [56].
The variables are expressed as (PB: large positive (big positive)), (PS: small positive (small positive)),(ZO: zero), (NS: slightly negative (small negative)), (NB: large negative (Big negative)). Table 2.1 shows the rules applied which ensure the relationship between the inputs and the output of the FL controller. The symmetric rule base is usually used for constant growth systems [66].

Table 2.1: Fuzzy rules

E	CE				
	NB	NS	ZO	PS	PB
NB	ZO	ZO	NB	NS	NS
NS	ZO	ZO	NB	NS	NS
ZO	NS	ZO	ZO	ZO	PB
PS	NS	PB	PS	ZO	ZO
PB	NB	NB	PB	ZO	ZO

2.4.3.3 defuzzification

The defuzzification uses the centroid method to calculate the output d_D which is considered as the barycenter [66].

2.5 Conclusion

In this chapter, we have begun with the most important and most delicate part of this study. This is the description of the DC/DC converter which is a power converter (DC/DC-Buck converter) controlled by an MPPT algorithm.
In the first part of this chapter, we presented the principle of direct connection between the photovoltaic generator and the load. Then we studied theoretically the operation of a Buck type converter which is used very often. The command of these converters is carried out by a variation in the duty cycle of the control signal of the switch which is produced from the MPPT algorithm. The second part is devoted to the explanation of the principle of MPPT research.
the study of the different MPPT algorithms used in our work, the method of Perturbation and Observation, Fuzzy Logic, and Artificial Neural Networks.
However, the simulation of these types of algorithms is the objective of the next chapter.

Chapter 3

Simulation and realisation of the PV system

3.1 Introduction

In the previous chapter , we explained how to control MPPT with the algorithms that were also explained , now in this last chapter we will do the simulation and realization of the PV system To carry out this order, we opted for a digital electronics based on a microcontroller, knowing that it contains several advantages, such as:
- Fewer components mean less weight, cost, and space are required.
- Their application is adaptable: the adjustment parameters can be changed by programming, ideally merely by changing the analog regulation's wiring.
- The algorithm in use might be made better.
- The capacity to use complex algorithms.
- The dynamics of the system (delay) may be impacted by the calculation times of the employed algorithms.

3.2 Description of the system

The following photovoltaic system connected to the converter (buck converter) is made using the MPPT algorithm(fuzzy or P&O or ANN) controller Element consisting of two units, the measurement unit, the control unit and a storage battery where the following diagram shows The Shape of the photovoltaic system Figure 3.1 [68].

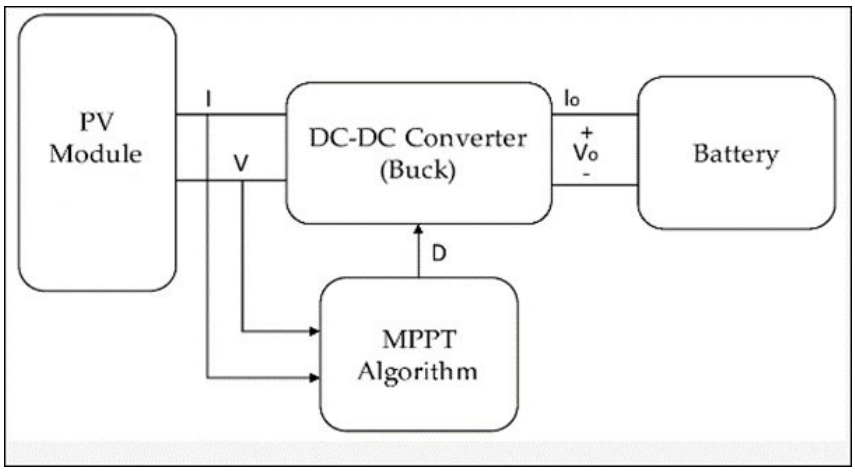

Figure 3.1: Block diagram of the photovoltaic (PV) system

3.2.1 GPV photovoltaic generator module

The technical characteristics of the GPV used in our project are given in the table (1.1),It is a module of 18 poly crystalline silicon cells in series, with a maximum power of 59.4 W.

3.2.2 BUCK Static Converter Design

Schematic for a GPV-Powered Buck Converter is given by the figure 3.2 [69].

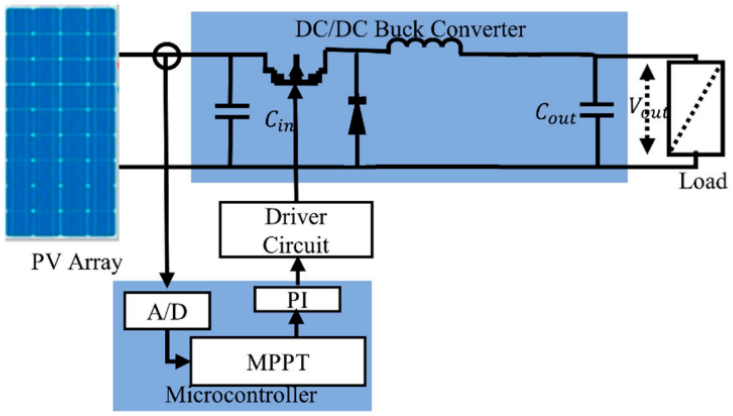

Figure 3.2: Schematic for a GPV-Powered Boost Converter

3.2.2.1 Calculation and selection of converter components

In this part, we will size the different components that make up the power circuit, namely, the L-smoothing inductor, the switching transistor, the capacitances and the diode. Determining these characteristics is a critical step in the implementation of an MPPT-controller Boost. The choice of elements is made considering that the converter is in Continuous Conduction Mode [40].

A.Transistor

The transistor must be sized to withstand the maximum current delivered to the load. We choose a MOSFET "IRFZ 44N"This MOSFET can operate with a voltage VDSS up to 50V, and a maximum current of up to 41A. It can also operate at a frequency of 100kHz (see ANNEX), in our realization, the operating frequency is 20kHz The choice of a switching frequency of 50kHz was motivated by the following reasons:
-The greater the switching frequency, the smaller the size of the reactive components used

(capacitances and inductance).
-The delay of the output with respect to the input which is due to the switching time is small ($4\mu c$). [40]

B.Diode

Fastness and the ability to tolerate the maximum current sent to the load are requirements for the diode to be employed. Its function is to stop the load's current from returning. Here, we installed a diode.
$P6KE36CA$: The P6KE Series is designed specifically to protect sensitive electronic equipment from voltage transients induced by lightning and other transient voltage events [70] (see ANNEX).
$UE4007$: UF4007 is a fast recovery diode with a continuous reverse voltage rating of 1000V and is suitable for forward currents of up to 1A. The UF4007 diode has a reverse recovery time of 75 ns. The diode is ideal for use in power supplies and switched voltage converter circuits [71] see ANNEX.
$IN4148$:For this IN4148 Diode, the maximum capacity for carrying current is 300mA it can resist up to 2A. This diode has 8ns of quick recovery time at 10mA of a forward current; so this diode is applicable where fast switching is required [72] (see ANNEX).

C.Inductor

This element is the most difficult to determine. Indeed, an inductance that is too low does not allow the operation of the power board, and an inductance that is too high, for its part, would cause significant power losses by the Joule effect.the inductance of the Buck circuit is calculated for a frequency of 20kHz and a ripple current of 0.5 A and Ripple voltage 0.12 V [40]
$V_{ripple} = V_{OUT} * 1\%$
$I_{ripple} = I_{OUT} * 10\%$
$V_{out} = 12V$
$V_{in} = 22.2V$
The value of the inductance is given by :

$$L = \frac{V_o(V_i - V_o)}{f_{sw} * I_{ripple} * V_i} \tag{3.1}$$

f_{sw} is the switching frequency, and V_{OUT} the charging voltage.

The ripple of the current I_{ripple}= 0.5A is chosen, so the value of the inductance L is :

$$L = \frac{12(22.2 - 12)}{20000 * 0.5 * 0.12} = 102.2mH \tag{3.2}$$

D. Capacitor C1 and C2

We place chemical capacitors at the input and output to filter out variations in input and output voltages. The capacitance values are calculated based on the desired corrugation as well as the desired average quantities. To meet the ripple condition of the output voltage, the capacitance of the capacitor C2 must verify the expression [40]:

$$C_2 \geq \frac{I_{ripple}}{8V_{ripple}f_{swiching}} \tag{3.3}$$

With:
$V_{ripple} = V_{OUT} * 1\%$ $V_{out} = 12v$ so $V_{ripple} = 0.012v$
$I_{ripple} = I_{OUT} * 10\%$ $I_{OUT} = P/V_{out}$=60/22.2=2.70 A so $I_{ripple} = 0.27A$
$f_{swiching} = 20Khz$

$$C_2 \geq 0.000140$$

To obtain the desired input voltage ripple, the capacitance of capacitor C1 must verify the expression:

$$C_1 \geq \frac{I_{pv}}{\Delta V_{pvmax}f_{swiching}} \tag{3.4}$$

$$C_1 \geq \frac{3.27}{0.006 * 20000} \tag{3.5}$$

$$C_1 \geq 0.02725$$

E. Resistance

In practice, the selected resistance value should be at least 6% higher than the theoretically calculated one. Therefore, the resistance value that will be used will be R=2.55 ohms.

$$V_{out} = RI_{OUT} \tag{3.6}$$

so $R = \frac{V_{out}}{I_{OUT}}$ $R = \frac{12}{5}$ $R = 2.4\Omega$

3.3 Realization of the system

The diagram below shows our prototype to be made, simulated under Proteus and simulated under EasyEDA. Our prototype has three distinct parts:
1)-Power Circuit That Encompasses, The Buck Chopper And Load.
2)-Arduino UNO Board Based Control Circuit
3)-The display of the results on the display LCD 20*02

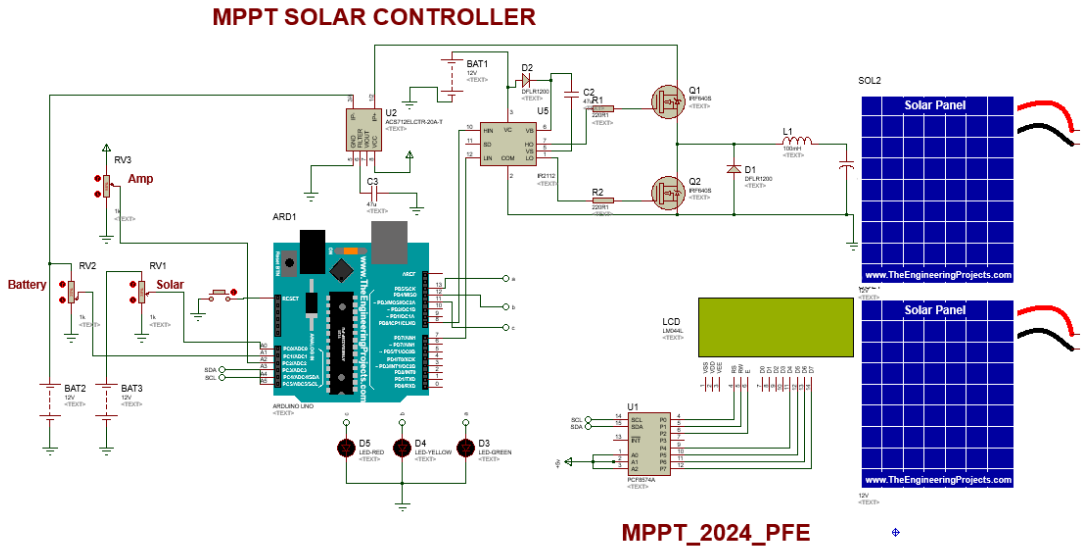

Figure 3.3: Simulation under Proteus

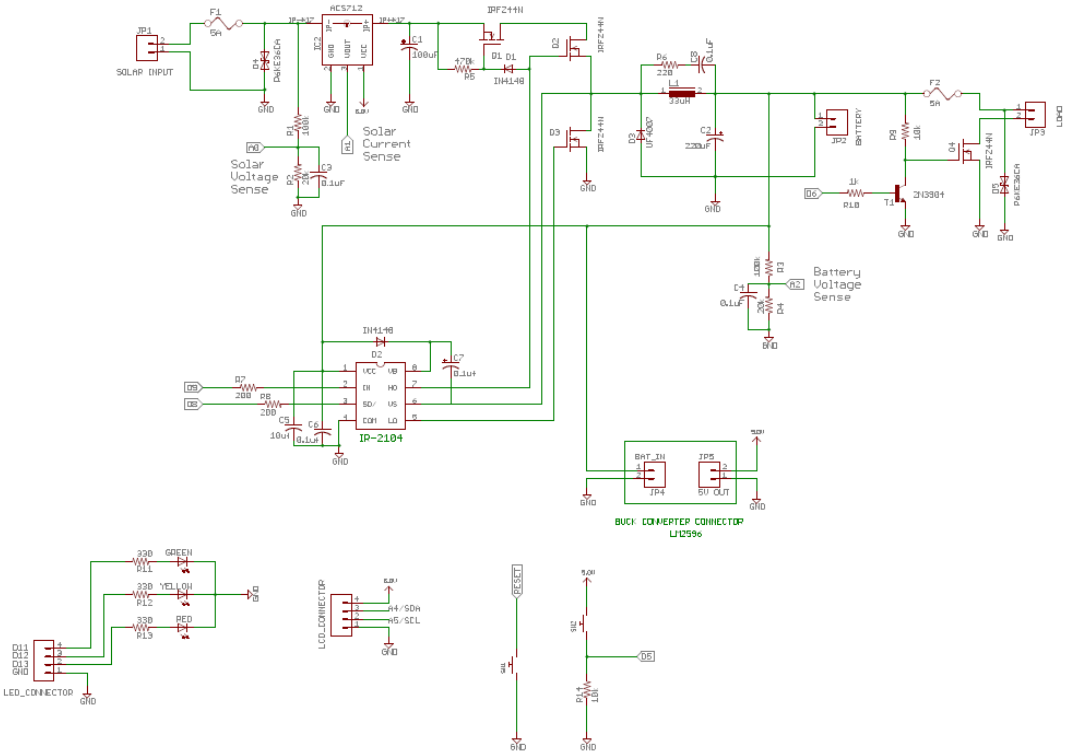

Figure 3.4: Simulation under EasyEDA

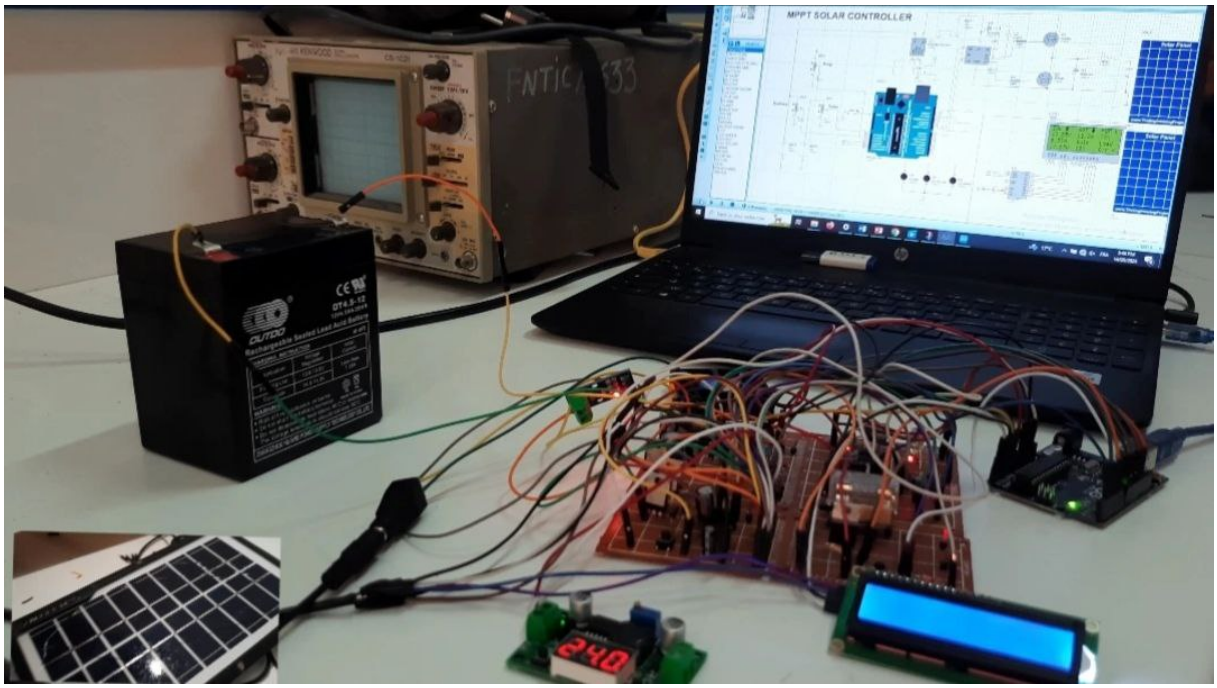

Figure 3.5: Overall Schematic of our prototype

3.3.1 The unit of measurement

For MPPT, several types of sensors are needed: current sensor, voltage sensor, Temperature sensor, etc. But in our work, only two sensors are needed : Current sensor and voltage sensor.

3.3.1.1 current sensor ACS712-5A

For the current measurement, we used the Hall effect current sensor of type ACS712 which provides us with an exploitable voltage. ACS712 current sensors have different measurement ranges of 5A, 20 and 30. The only difference between these measurement ranges is in their sensitivity. In our project we used the ACS712ELC-5A current sensor [73], which measures the current going +5A and that we have found to have a sensitivity of 185mV/A (see ANNEX). The ACS712 current sensors generate an output voltage that is

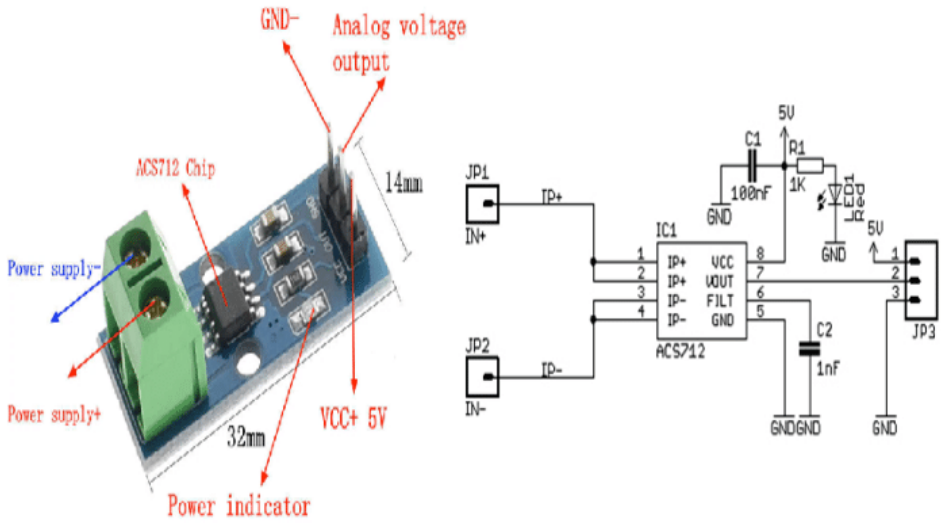

Figure 3.6: Current sensor ACS712ELCTR -05B-T

directly proportional to the current flowing through the circuit. It is an active device which means that it needs a Vcc voltage power supply for its operation. In no-load operation, the output voltage is equal to 677/2 and when the load is connected, the output voltage is equal to [1] :

$$V_{out}(V) = \frac{V_{cc}(V)}{2} + Sensibilit(\frac{mV}{A}) * courant(A) \tag{3.7}$$

The value, Vcc/2 is the offset of our sensor which compensates for the instantaneous negative values of the current, so we have at the output of the current sensor a voltage that varies between 0V and 5V.

3.3.1.2 voltage sensor

The measurement of the voltage is necessary to calculate the power produced by the photovoltaic generator, although the voltage to be measured for our application does not exceed the threshold of tolerance of the Arduino board. However, the voltage to be measured for our application exceeds the tolerance threshold which is 5V. A voltage higher than 5V may destroy the Arduino board. To avoid this, it is advisable to use a voltage divider, which will lower the voltage to be measured. the tolerance threshold of the Arduino. The output voltage of the divider is given by the formula next:

$$V_{out} = \frac{R_2}{R_2 + R_1} V_{pv} \tag{3.8}$$

If we admit that the maximum voltage delivered by the GPV is 18 V. In our work, the values of R2 and R1 are 28 $k\Omega$ and 72$k\Omega$ respectively [40].

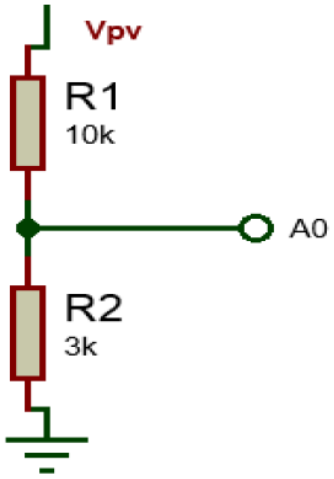

Figure 3.7: voltage sensor

3.3.2 The unit of control

The unit of control is the unit of decisions. Its role is to perform the corresponding calculations and control the BUCK switch by an MPPT algorithm. In practice, all of this can be accomplished through the use of a microcontroller. We chose the Arduino UNO board.

3.3.2.1 Arduino UNO

1. Definition

Arduino Uno is a microcontroller board grounded on the ATmega328 . It has 6 analog

inputs, a 16 MHz ceramic resonator, 14 digital input/output pins (6 of which can be used as PWM outputs), a USB connector, a power jack, an ICSP header, and a reset button. Its designs include features that benefit the microcontroller in every manner conceivable. To begin using it, just use a USB cable to connect it to a computer, or use an AC-to-DC adapter or battery to power it [74, 75].

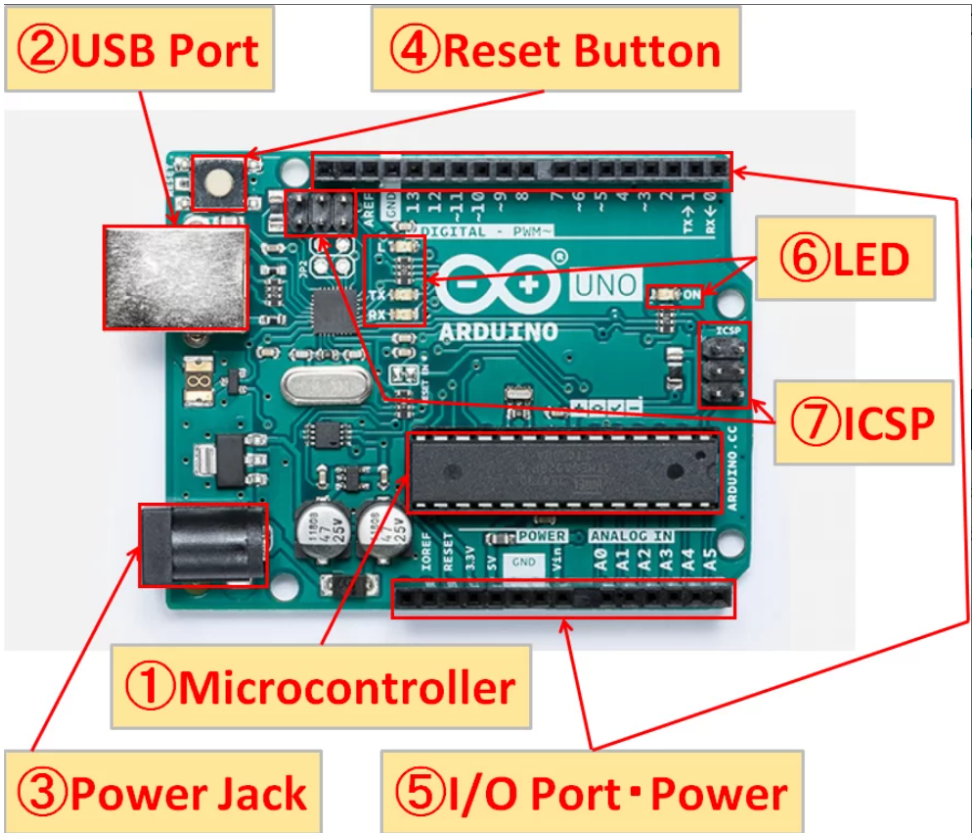

Figure 3.8: Presentation of the Arduino uno board

This card features:

-14 digital I/O pins (14 of which can be used as PWM (PWM) outputs.

-6 analog inputs.

-4 UART (Universal Asynchronous Receiver-Transmitter).

-16 Mhz crystal.

-a USB connection.

-a power connector jack.

-an ICSP (in-circuit programming) connector.

-a reset button.

2. Arduino UNO Board Specifications

Table 3.1: Arduino UNO Board Specifications

Microcontroller	ATmega328
Operating Voltage	5V
Input Voltage (recommended)	7-12V
Digital I/O Pins	14 (of which 6 provide PWM output)
Analog Input Pins	6
DC Current per I/O Pin	40 mA
DC Current for 3.3V Pin	50 mA
Flash Memory	32 KB (ATmega328) of which 0.5 KB used by bootloader
SRAM	2 KB (ATmega328)
EEPROM	1 KB (ATmega328)
Clock Speed	16 MHz

3.3.3 other electronics components

3.3.3.1 LCD "16*2"

This is interface, 16 * 2 LCD module, a new high-quality 2-line,16 character LCD module with on-board Adjust contrast control, backlight , it was used to display the values of voltage, current, and power(see ANNEX).

3.3.3.2 Driver "IR-2104"

It is a half-bridge driver, the IR2104 IC. Low-power input is accepted, and high-current drives are output. Similar to a power MOSFET, it supplies power to a high-power transistor's gate. The IR2104 gate driver also has additional capabilities as a power amplifier and a level shifter (see ANNEX).

3.3.3.3 Step-down Converter Module "LM 2596"

LM 2596 is a monolithic and integrated circuit that provides all the active functions of a step-down Switch regulator (buck), capable of driving a 3A load with excellent line and Load Regulation (see ANNEX).

3.4 simulation

building a simulation in MATLAB that combines artificial neural networks, fuzzy logic, and P&O algorithms.Target parameters, which include system inputs like temperature

and light intensity as well as target outputs like the produced electrical power, can be chosen for control.A P&O method that determines changes in the angle of inclination based on the generated electrical power can be implemented using MATLAB.further to use fuzzy logic to intelligently modify the system parameters in response to a variety of environmental variables.The best result can be predicted by using an artificial neural network (ANN) to learn the patterns of temperature and lighting. This solution entails utilizing Simulink's functionalities. The block diagram in Simulink is represented by the form 3.9

3.4.1 Simulink The block diagram general

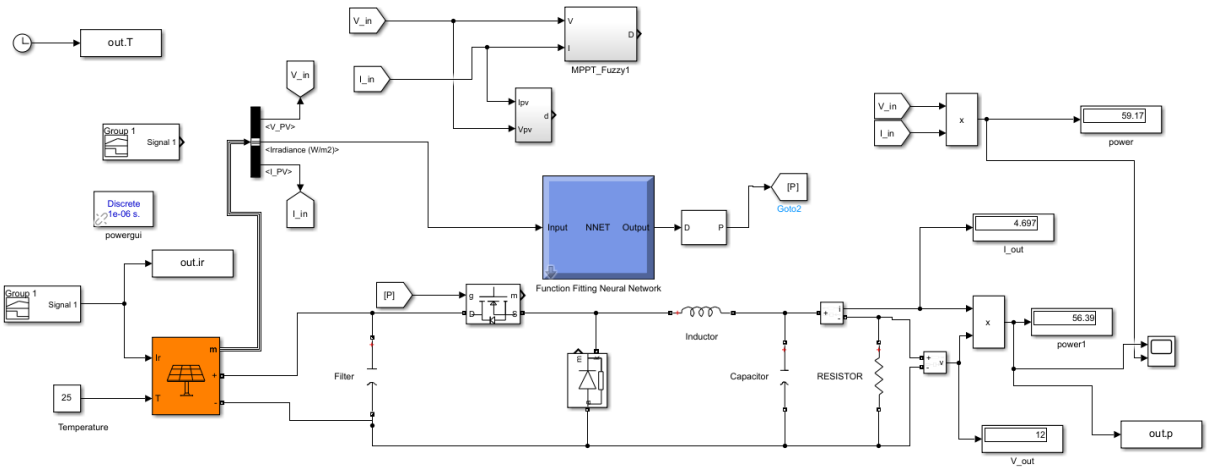

Figure 3.9: The block diagram general of matlab

Where there was a change in radiation in six stages, the radiation value starts from 542 to 562 to 611 to 865 to 918 to 1000 W/m^2
This plot is represented the change in radiation by the form 3.10

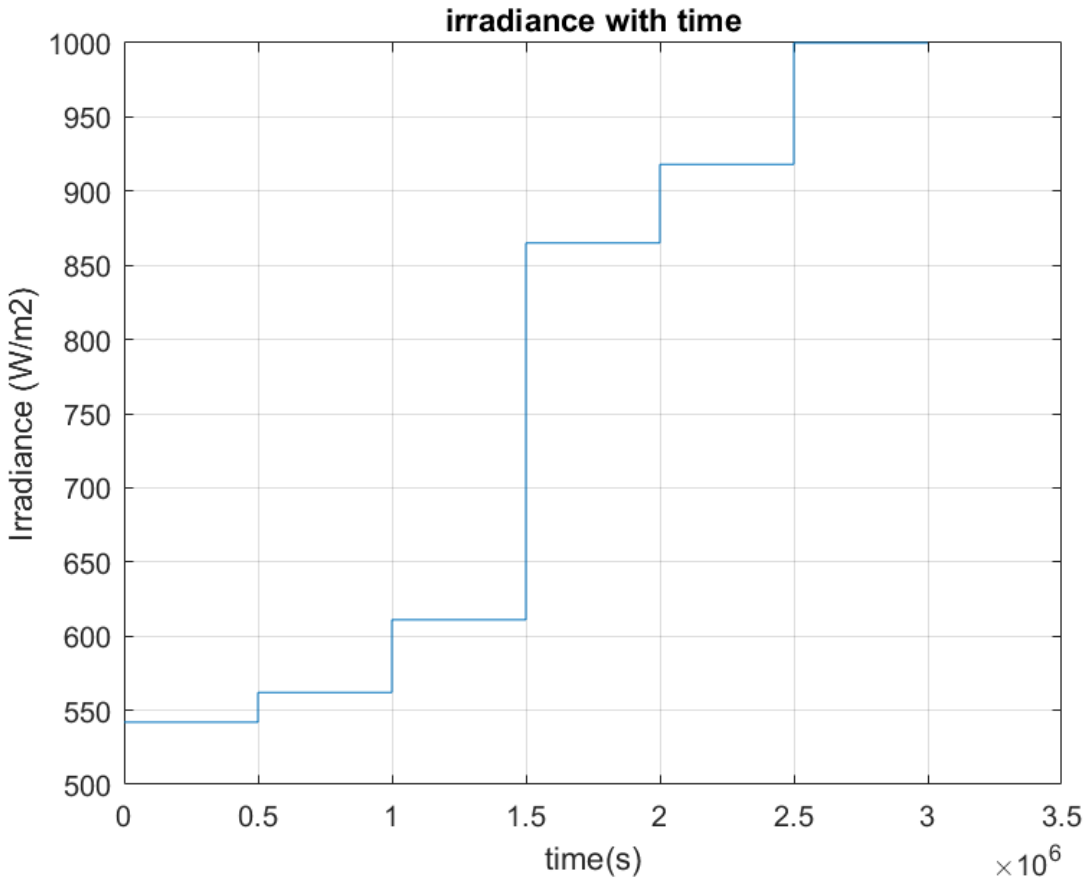

Figure 3.10: The block diagram the change in radiation in matlab

3.4.1.1 The block diagrams of the algorithm P&O:

The simulation calculates the step size (step size) and the solar module's capacity data over a certain time period. To replicate the process, an iterative loop is employed. The current and prior voltages are assessed at each repetition to decide whether to increase or decrease

3.4.1.2 result and discussion of algorithm p&o

The tracking efficiency according to the standard conditions in the P&o algorithm was obtained with an estimated value of 99.88% with an estimated response time value of 5.23%

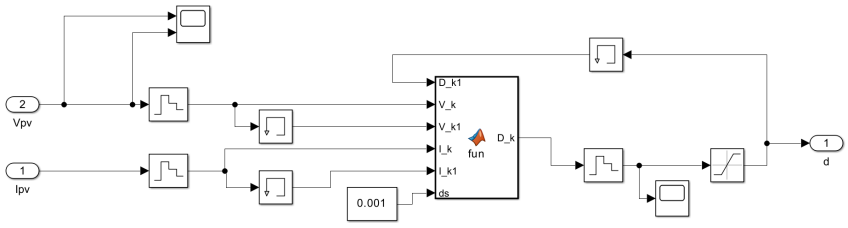

Figure 3.11: Block diagram of the P&O algorithm

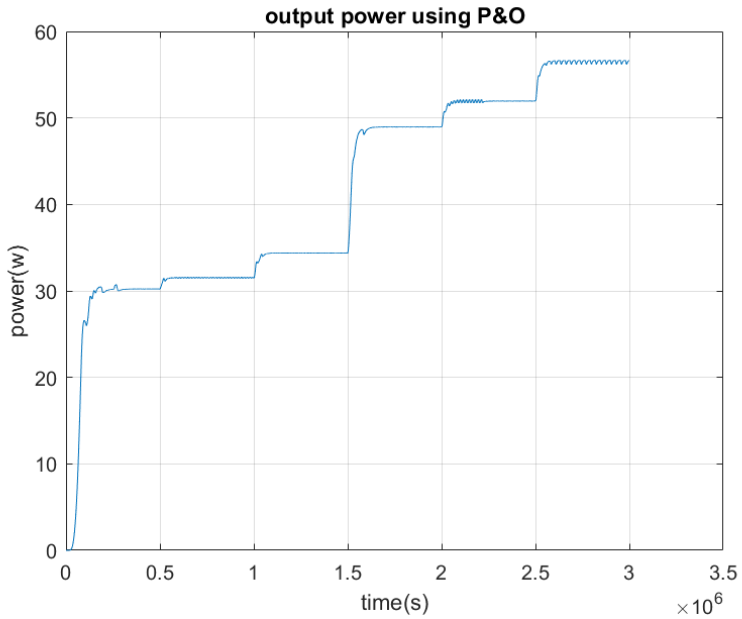

Figure 3.12: output power of algorithm p&o

3.4.1.3 The block diagrams of the algorithm ANN:

Provide the desired amount of data for the neural network's training. Input and output data must be compatible with the issue you want to use ANN to solve. Select the right neural network architecture, taking into account the number of layers and modules in each layer. Train the model using the data.

3.4.1.4 result and discussion of algorithm ANN

The tracking efficiency according to the standard conditions in the ANN algorithm was obtained at a value of 99.98% with an estimated response time value of 3.66%

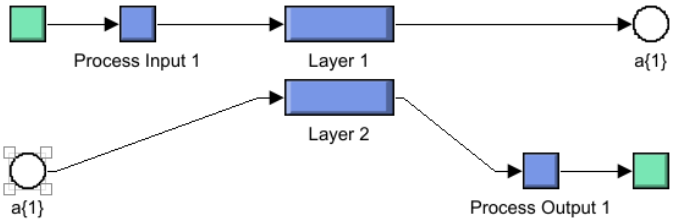

Figure 3.13: Block diagram of the ANN algorithm

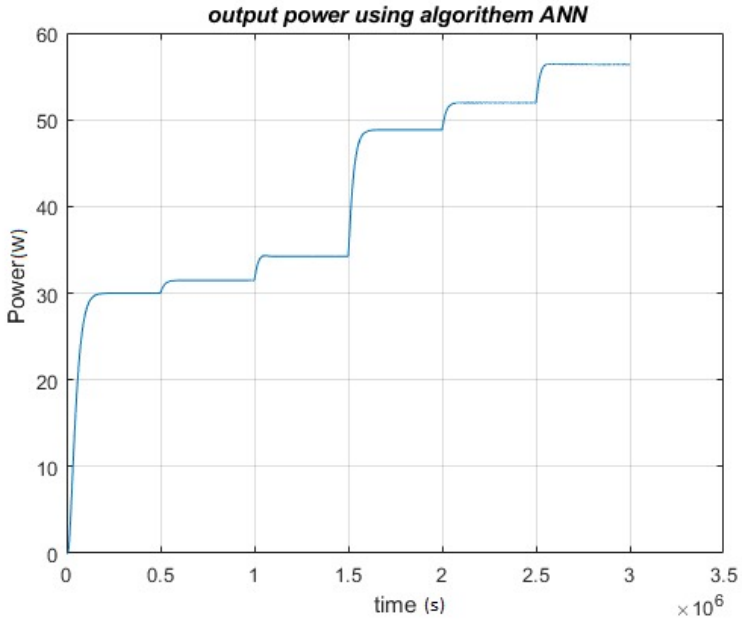

Figure 3.14: output power of algorithm ANN

3.4.1.5 The block diagrams of the algorithm FLC:

Write fuzzy rules that obliquely explain the system's behavior and define fuzzy variables.The way the system reacts to various inputs is determined by these rules. Make a Membership Function transition function. Apply the data to fuzzy logic. Compare the outcomes with the predicted values to assess the fuzzy model's performance.

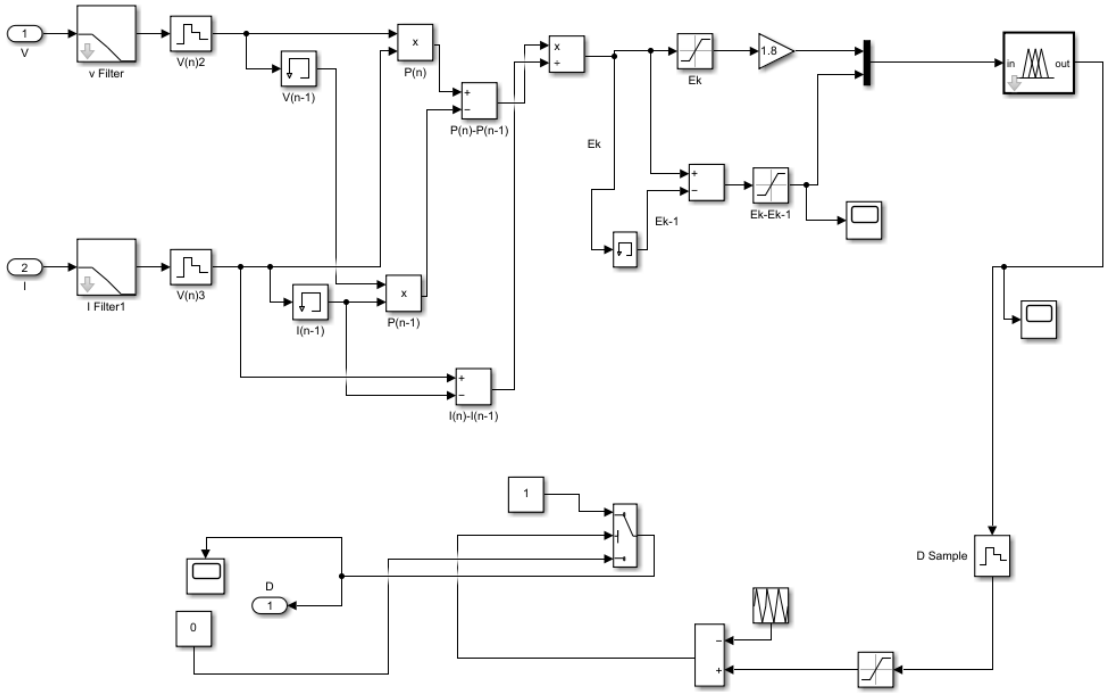

Figure 3.15: Block diagram of the FLC algorithm

3.4.1.6 result and discussion of algorithm FLC

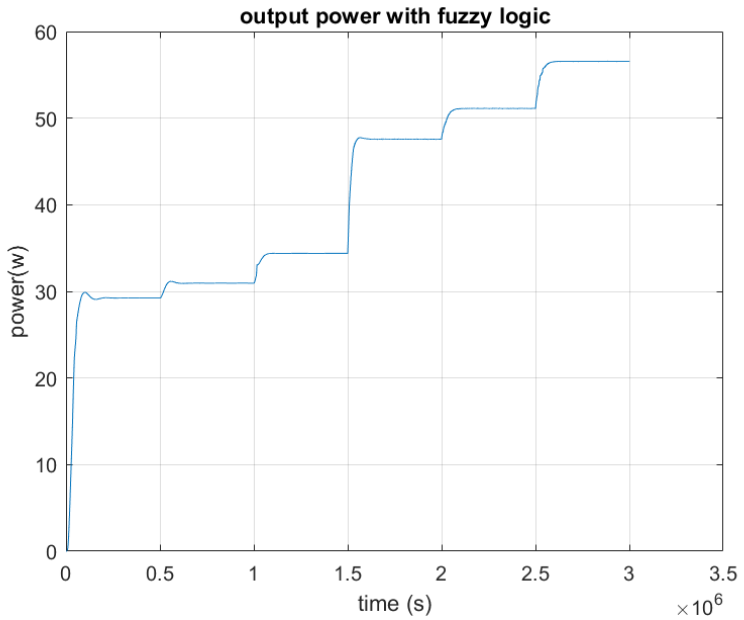

Figure 3.16: output power of algorithm Fuzzy logic

The tracking efficiency was obtained according to the standard conditions in the fuzzy

logic algorithm, estimated at 99.98% with an estimated response time of 4.33%

3.4.1.7 Discussion of three algorithms

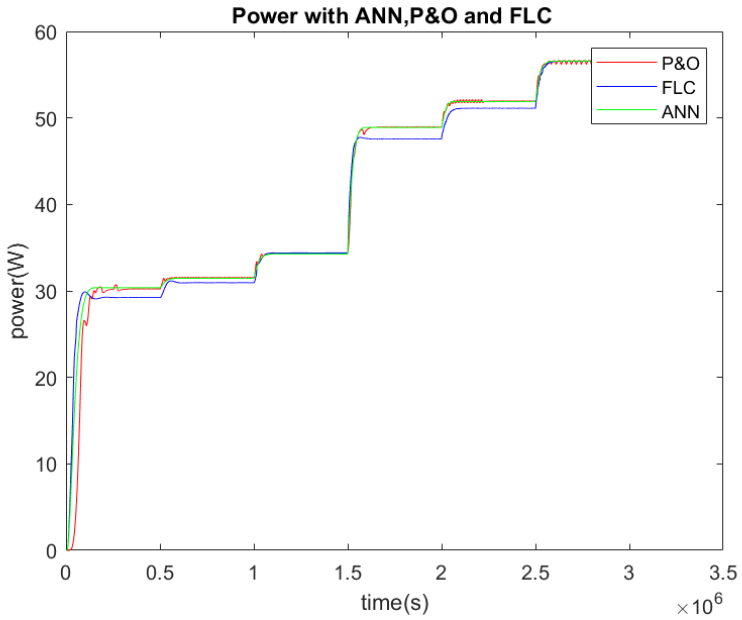

Figure 3.17: output power of three algorithms P&O.FLC and ANN

As we note in this work, better response time results were obtained in the artificial neural network algorithm than the fuzzy logic algorithm and the disturbance and control algorithm, and we also noticed that the ANN algorithm and the P&O algorithm are better than the fuzzy logic algorithm in the first half of the radiation change, and in the middle the fuzzy logic is better and after the middle we notice better results in the ANN algorithm and the Fuzzy Logic on P&O

3.5 Conclusion

This chapter covers the simulation and implementation of a PV system driven by three different MPPT algorithm variants using PROTEUS. Included in the system are a solar generator, a DC-DC converter (Buck), an Arduino UNO board for system control, a resistive load, current and voltage sensors, and an LCD display for real-time results presentation.

It can be concluded that, with the three algorithms, the PV panel can provide the maximum power. However, the performance of Artificial Neural Networks MPPT is better than Fuzzy logic algorithm and traditional algorithms (P&O) ,and fuzzy logic algorithms is better than the algorithm (P& O) for nonlinear systems , has the ability to reduce the turbulent voltage when the MPPT was recognized. This action directly preserves a more stable output power compared to conventional MPPT where the output power fluctuates around MPP.The tracking efficiency was obtained according to the standard conditions in the Ann algorithm with a value of 99.98% better than the fuzzy logic algorithm, where the tracking efficiency in the standard conditions achieved an estimated value of 99.98% and also better than the disturbance and monitoring algorithm, thus achieving tracking efficiency in the standard conditions an estimated value of 99.88%, and the artificial neural network algorithm achieved an estimated response time value of 3.66% better than fuzzy logic, which achieved an estimated response time of 4.33% the P&O algorithm that achieved the response time value is estimated at 5.23%

Conclusion Générale

The work presented in this thesis deals with the simulation, optimization, and implementation of a photovoltaic system powered by a buck transformer. This converter has the advantage of being a voltage booster that allows this system to adapt to weather changes and extract the maximum power available for loading

Measurements carried out under real conditions using a solar panel made it possible to determine the I-V and P-V characteristics of the panel. A detailed model under Proteus has been developed to represent the main characteristics of the PV panel. This model has been validated by comparing the simulation results with the experimental measurements Simulations and experimental results showed the interest of the device in finding the maximum power. Algorithms, p& o (perturbation and observation), fuzzy logic and the use of an artificial neural network using the microcontroller MPPT The Arduino Uno board, in order to determine the operating point with the maximum power of the photovoltaic panel and acts as a system controller.

Based on the simulation and experimental results, it can be concluded that using the three algorithms, the photovoltaic panel can provide maximum power. However,the performance of MPPT on an artificial neural network, fuzzy logic and (P& O) is more powerful, accurate and with efficiency , for nonlinear systems, it has the ability to reduce the loss and disturbance of power when the MPPT is recognized , to cope with jamming and improve system performance.

As we mentioned earlier in our study on the following topics Experimental implementation of a novel scheduling algorithm for adaptive and modified P&O MPPT controller using fuzzy logic for WECS Where they achieved an efficiency of 99.47% and also in a study MPPT implementation and simulation using developed P&O algorithm for photovoltaic system concerning efficiency They achieved an efficiency of 99.83% and also in terms of response time achieved a study An efficient Fuzzy Logic MPPT Control Approach for Solar PV System : A Comparative Analysis with the Conventional Perturb and Observe Technique 6% compared to what was obtained in this work, the tracking efficiency is higher than the previous three studies in the standard conditions of the three algorithms

to the maximum value estimated at 99.98%, and we also achieved a lower response time compared to the previous three studies by 3.66%

Regarding the prospects of this work, we can mention:

- Apply these MPPT optimization algorithms to other types of load in other systems
- Use metaheuristic optimization techniques such as genetic algorithms, particle swarm optimization (PSO) to optimize the work cycle in real time.
- Boost voltage converter can be used instead of buck converter in case of voltage raising

Bibliography

[1] Razieh Khanaki, M. A. M. Radzi, and M. Hamiruce Marhaban. Comparison of ann and po mppt methods for pv applications under changing solar irradiation. In *2013 IEEE Conference on Clean Energy and Technology (CEAT)*, pages 287–292, 2013.

[2] P Ganesh, G Raju Kumar, S Sharanya Reddy, and R Srinivas Reddy. Fuzzy logic control of mppt controller for pv system. *Journal of Engineering Sciences*, 14(06), 2023.

[3] Saibal Manna, Deepak Kumar Singh, Ashok Kumar Akella, Hossam Kotb, Kareem M AboRas, Hossam M Zawbaa, and Salah Kamel. Design and implementation of a new adaptive mppt controller for solar pv systems. *Energy Reports*, 9:1818–1829, 2023.

[4] Dhananjay Choudhary and Anmol Ratna Saxena. Dc-dc buck-converter for mppt of pv system. *International Journal of Emerging Technology and Advanced Engineering*, 4(7):813–821, 2014.

[5] Jaldeep Kumar, Bhuvnesh Rathor, and Prakash Bahrani. Fuzzy and po mppt techniques for stabilized the efficiency of solar pv system. In *2018 International Conference on Computing, Power and Communication Technologies (GUCON)*, pages 259–264, 2018.

[6] Ahteshamul Haque. Maximum power point tracking (mppt) scheme for solar photovoltaic system. *Energy Technology & Policy*, 1(1):115–122, 2014.

[7] Amir Hussain, Avanish Kumar, and Laxmidhar Behera. Sliding mode control of a buck converter for maximum power point tracking of a solar panel. In *2013 IEEE International Conference on Control Applications (CCA)*, pages 661–666, 2013.

[8] T Laagoubi, M Bouzi, and M Benchagra. Analysis and comparaison of mppt nonlinear controllers for pv system using buck converter. *International Journal of Engineering Research & Technology (IJERT)*, 4(11), 2015.

[9] Karima Boudaraia, Hassane Mahmoudi, Ahmed Abbou, and Mohamed Hilal. Buck converter mppt control of a photovoltaic system. In *2016 5th International Conference on Multimedia Computing and Systems (ICMCS)*, pages 783–787, 2016.

[10] Parag K. Atri, P. S. Modi, and Nikhil Shashikant Gujar. Comparison of different mppt control strategies for solar charge controller. In *2020 International Conference on Power Electronics IoT Applications in Renewable Energy and its Control (PARC)*, pages 65–69, 2020.

[11] Dhananjay Choudhary and Anmol Ratna Saxena. Dc-dc buck-converter for mppt of pv system. *International Journal of Emerging Technology and Advanced Engineering*, 4(7):813–821, 2014.

[12] Lahcen El Mentaly, Abdellah Amghar, and Hassan Sahsah. Comparison between hc, focv and tg mppt algorithms for pv solar systems using buck converter. In *2017 International Conference on Wireless Technologies, Embedded and Intelligent Systems (WITS)*, pages 1–5, 2017.

[13] Barnam Jyoti Saharia, Munish Manas, and Subir Sen. Comparative study on buck and buck-boost dc-dc converters for mpp tracking for photovoltaic power systems. In *2016 Second International Conference on Computational Intelligence Communication Technology (CICT)*, pages 382–387, 2016.

[14] Prisma Megantoro, Yabes Dwi Nugroho, Fajar Anggara, Aji Pakha, and Brahmantya Aji Pramudita. The implementation of genetic algorithm to mppt technique in a dc/dc buck converter under partial shading condition. In *2018 3rd International Conference on Information Technology, Information System and Electrical Engineering (ICITISEE)*, pages 308–312, 2018.

[15] R Arulmurugan and N Suthanthira Vanitha. Intelligent fuzzy mppt controller using analysis of dc to dc novel buck converter for photovoltaic energy system applications. In *2013 International Conference on Pattern Recognition, Informatics and Mobile Engineering*, pages 225–231. IEEE, 2013.

[16] Asaad AH AlZubaidi, Laith Abdul Khaliq, Hassan Salman Hamad, Waleed Khalid Al-Azzawi, Mohanad Sameer Jabbar, and Thaer Abdulwahhab Shihab. Mppt implementation and simulation using developed p&o algorithm for photovoltaic system concerning efficiency. *Bulletin of Electrical Engineering and Informatics*, 11(5):2460–2470, 2022.

[17] Khaled Osmani, Ahmad Haddad, Thierry Lemenand, Bruno Castanier, and Mohamad Ramadan. An investigation on maximum power extraction algorithms from pv systems with corresponding dc-dc converters. *Energy*, 224:120092, 2021.

[18] Shamrat Bahadur, Kalyan Mondol, Ashif Mohammad, Farhana Mahjabeen, Tamzeed Al-Alam, and Md Bulbul Ahammed. Design and implementation of low cost mppt solar charge controller. 2022.

[19] Hicham Gouabi, Abdeldjebar Hazzab, Mohamed Habbab, Miloud Rezkallah, and Ambrish Chandra. Experimental implementation of a novel scheduling algorithm for adaptive and modified p&o mppt controller using fuzzy logic for wecs. *International Journal of Adaptive Control and Signal Processing*, 35(9):1732–1753, 2021.

[20] Ahmed M Atallah, Almoataz Y Abdelaziz, and Raihan S Jumaah. Implementation of perturb and observe mppt of pv system with direct control method using buck and buck-boost converters. *Emerging Trends in Electrical, Electronics & Instrumentation Engineering: An international Journal (EEIEJ)*, 1(1):31–44, 2014.

[21] Mounir Dabboussi, Ali Hmidet, and Olfa Boubaker. An efficient fuzzy logic mppt control approach for solar pv system: A comparative analysis with the conventional perturb and observe technique. In *2020 6th IEEE International Energy Conference (ENERGYCon)*, pages 366–371, 2020.

[22] Djazira DRAIDI. Réalisation d'un chargeur de batterie basé sur la commande mppt photovoltaïque. 2022.

[23] Ahmed HAKOUMI, Abdeldjalil BENAMAR, Touhami GHITAOUI, et al. *Commande MPPT et contrôle d'un systemephotovoltaique 3KW par la logique floue*. PhD thesis, Université Ahmed Draïa-Adrar, 2019.

[24] Fatiha ABDELLI and Souad BAALI. *Nouvelle approche du MPPT adaptatif utilisé dans le Système Photovoltaïque*. PhD thesis, UNIVERSITE AHMED DRAIA-ADRAR, 2023.

[25] Muhammad Hilman Hakimi Yunus and Suhaimi Saiman. Enhancing solar smartphone charger efficiency through mppt technology. *Evolution in Electrical and Electronic Engineering*, 5(1):139–148, 2024.

[26] Goksel Gokkus. Anfis-based improved gwo: Rapid prototyping of low-power solar energy system under fast-changing solar radiation conditions. *Journal of Radiation Research and Applied Sciences*, 17(2):100920, 2024.

[27] Linda Johnsana et al. Comparative analysis of improved efficient converter topologies with mppt techniques for battery charging using photovoltaic arrays in electric vehicle applications.

[28] Nivedita Kshatri et al. An innovate on hybrid power generation on dc–dc buck converter with mppt systems. *Turkish Journal of Computer and Mathematics Education (TURCOMAT)*, 11(3):1741–1758, 2020.

[29] Nicholas Apergis and James E Payne. Renewable and non-renewable energy consumption-growth nexus: Evidence from a panel error correction model. *Energy economics*, 34(3):733–738, 2012.

[30] Fiseha Mekonnen Guangul and Girma T Chala. Solar energy as renewable energy source: Swot analysis. In *2019 4th MEC international conference on big data and smart city (ICBDSC)*, pages 1–5. IEEE, 2019.

[31] Soufiane LATRECHE et al. Etude et réalisation d'un système photovoltaïque à base d'une carte arduino uno. 2016.

[32] Alaeddine AHMED. *CONTRIBUTION AU DEVELOPPEMENT D'UN OUTIL D'AIDE AU DIAGNOSTIQUE DE PERFORMANCES DES 'MPPT'DANS LA CHAINE DE CONVERSION PHOTOVOLTAIQUE.* PhD thesis, Université de M'Sila-Mohamed Boudiaf.

[33] Younes BOUTERAA. Commande d'un système de pompage photovoltaïque. 2021.

[34] Idris Bouchama and Melouki Dilmi. *PERFORMANCE STUDY OF InGaP/GaAs/Ge TANDEM SOLAR CELLS BY SIMULATION.* PhD thesis, 06 2016.

[35] Omar Saket. *Caractérisation électrique de nanofils de semi-conducteurs III-V pour des applications photovoltaïques.* PhD thesis, 07 2020.

[36] Djazira DRAIDI. Réalisation d'un chargeur de batterie basé sur la commande mppt photovoltaïque. 2022.

[37] Hani Rejdal and Boubekeur Encadreur Medjahed. *Optimisation du fonctionnement d'un champ photovoltaïque sous des conditions d'ombrage partiel.* PhD thesis, Université de Jijel, 2020.

[38] Hichem Bencherif. *Etude et modélisation analytique d'une cellule solaire à base de Si-Ge.* PhD thesis, 11 2015.

[39] Justyna Pastuszak and Paweł Węgierek. Photovoltaic cell generations and current research directions for their development. *Materials*, 15(16):5542, 2022.

[40] Fethallah Tati, Oussama BEN LAMOUDI, et al. *Etude et Réalisation d'unSystème Photovoltaïque Optimisé par Logique Floue*. PhD thesis, 2018.

[41] Sid Ahmed El Mehdi Ardjoun. *Commande d'un système d'énergies renouvelables Multisources relié au réseau électrique*. PhD thesis, 04 2016.

[42] Masafumi Yamaguchi, Kan-Hua Lee, Kenji Araki, Nobuaki Kojima, Hiroyuki Yamada, and Yasuhiro Katsumata. Analysis for efficiency potential of high-efficiency and next-generation solar cells. *Progress in Photovoltaics: Research and Applications*, 26(8):543–552, 2018.

[43] Ambadjigna Hervé SOMBORO, Ousmane SOUMAORO, and Maliki GUINDO. Modélisation, optimisation des paramètres et prédiction de la production du module pv byd255p6c-30 pour la centrale photovoltaïque de 33 mwc de ségou. *Afrique SCIENCE*, 19(6):89–101, 2021.

[44] Leila BOUCERREDJ. Modélisation et simulation d'un système photovoltaïque par la commande mppt. *Algerian Journal of Engineering Architecture and Urbanism*, 5(5):197–205, 2021.

[45] Djamil Boukhers and A Bouzid. Optimisation d'un système d'énergie photovoltaique. application au pompage. 2007.

[46] FZ Zerhouni, MH Zerhouni, M Zegrar, and A BOUDGHÉNE Stambouli. Recherche du maximum de puissance d'un générateur photovoltaique. *ACTA ELECTROTEHNICA*, 53(12):130–133, 2012.

[47] Barry W. Williams. Dc-to-dc converters with continuous input and output power. *IEEE Transactions on Power Electronics*, 28(5):2307–2316, 2013.

[48] Ebrahim Babaei and Mir Esmaeel Seyed Mahmoodieh. Systematical method of designing the elements of the cuk converter. *International Journal of Electrical Power & Energy Systems*, 55:351–361, 2014.

[49] JM Enrique, E Duran, M Sidrach-de Cardona, and JM Andujar. Theoretical assessment of the maximum power point tracking efficiency of photovoltaic facilities with different converter topologies. *Solar Energy*, 81(1):31–38, 2007.

[50] David J Irwin. *Academic Press Series in Engineering*. Academic Press, 2001.

[51] N Mazouz and A Midoun. Control of a dc/dc converter by fuzzy controller for a solar pumping system. *International Journal of Electrical Power & Energy Systems*, 33(10):1623–1630, 2011.

[52] Karima Boudaraia, Hassane Mahmoudi, Ahmed Abbou, and Mohamed Hilal. Buck converter mppt control of a photovoltaic system. In *2016 5th International Conference on Multimedia Computing and Systems (ICMCS)*, pages 783–787. IEEE, 2016.

[53] Dhananjay Choudhary and Anmol Ratna Saxena. Dc-dc buck-converter for mppt of pv system. *International Journal of Emerging Technology and Advanced Engineering*, 4(7):813–821, 2014.

[54] Electronics coach. https://electronicscoach.com/2024-05-14.

[55] Alaeddine AHMED. *CONTRIBUTION AU DEVELOPPEMENT D'UN OUTIL D'AIDE AU DIAGNOSTIQUE DE PERFORMANCES DES 'MPPT'DANS LA CHAINE DE CONVERSION PHOTOVOLTAIQUE.* PhD thesis, Université de M'Sila-Mohamed Boudiaf.

[56] Fathi Aashoor. *Maximum power point tracking techniques for photovoltaic water pumping system.* PhD thesis, University of Bath, 2015.

[57] Enzo Grossi and Massimo Buscema. Introduction to artificial neural networks. *European journal of gastroenterology & hepatology*, 19(12):1046–1054, 2007.

[58] Data flaire. https://data-flair.training/blogs/artificial-neural-networks-for-machine-learning/2024-05-14.

[59] machine learning mastery. https://machinelearningmastery.com/gentle-introduction-to-the-bias-variance-trade-off-in-machine-learning/2024-05-14.

[60] geeks for geek. https://www.geeksforgeeks.org/activation-functions-neural-networks/2024-05-15.

[61] Kunal Sandip Garud, Simon Jayaraj, and Moo-Yeon Lee. A review on modeling of solar photovoltaic systems using artificial neural networks, fuzzy logic, genetic algorithm and hybrid models. *International Journal of Energy Research*, 45(1):6–35, 2021.

[62] T Ttayagarajan, M Ponnavaikko, J Shanmugam, RC Panda, and PG Rao. Artificial neural networks: principle and application to model based control of drying systems-a review. *Drying technology*, 16(6):931–966, 1998.

[63] Sadeq D Al-Majidi, Maysam F Abbod, and Hamed S Al-Raweshidy. Design of an intelligent mppt based on ann using a real photovoltaic system data. In *2019 54th International universities power engineering conference (UPEC)*, pages 1–6. IEEE, 2019.

[64] Mahmoud Nour Ali. Improved design of artificial neural network for mppt of grid-connected pv systems. *2018 Twentieth International Middle East Power Systems Conference (MEPCON)*, pages 97–102, 2018.

[65] Shruti Kambalimath and Paresh Chandra Deka. A basic review of fuzzy logic applications in hydrology and water resources. *Applied Water Science*, 10(8):1–14, 2020.

[66] Nedjma Aouchiche. *Conception d'une commande MPPT optimale à base d'intelligence artificielle d'un système photovoltaïque.* PhD thesis, Université Bourgogne Franche-Comté, 2020.

[67] Nasir Selman. Comparison between perturb observe, incremental conductance and fuzzy logic mppt techniques at different weather conditions. *International Journal of Innovative Research in Science, Engineering and Technology*, 5:12556–12569, 07 2016.

[68] Carlos Robles, John Taborda Giraldo, and Omar Rodriguez Alvarez. Fuzzy logic based mppt controller for a pv system. *Energies*, 10(12):2036, 2017.

[69] A Comprehensive Review on a PV Based System to Harvest Maximum Power - Scientific Figure on ResearchGate. Available from: https://www.researchgate.net/figure/The-buck-boost-converter-with-a-PV-module$_fig13_{3}37762507/2024 - 05 - 15$.

[70] https://www.littelfuse.com/products/tvs-diodes/leaded/p6ke/p6ke36ca.aspx]/2024-05-15.

[71] https://www.majju.pk/product/uf4007-diode-general-purpose-ultra-fast/2024-05-16].

[72] https://www.elprocus.com/1n4148-diode/2024-05-16].

[73] Shereefdeen Sanni, Kehinde Olusuyi, and Ismail MAhmud. Design and implementation of home appliance energy monitoring device. 06 2019.

[74] N. Sathish Kumar, B. Vuayalakshmi, R. Jenifer Prarthana, and A. Shankar. Iot based smart garbage alert system using arduino uno. In *2016 IEEE Region 10 Conference (TENCON)*, pages 1028–1034, 2016.

[75]

Appendix A

ALL Datasheet

.
.
.
.
.
.
.
.

CHONGQING PINGYANG ELECTRONICS CO.,LTD.

UF4001 THRU UF4007

ULTRAFAST RECTIFIER

VOLTAGE：50-1000V **CURRENT：1.0A**

FEATURES

- Low power loss, high efficiency
- Low leakage
- Low forward voltage
- High current capability
- High speed switching
- High surge capability
- High reliability

MECHANICAL DATA

- ***Case***: Molded plastic
- ***Epoxy***: UL94V-0 rate flame retardant
- ***Lead***: MIL-STD- 202E, Method 208 guaranteed
- ***Polarity***:Color band denotes cathode end
- ***Mounting position***: Any
- ***Weight***: 0.33 grams

DO-41

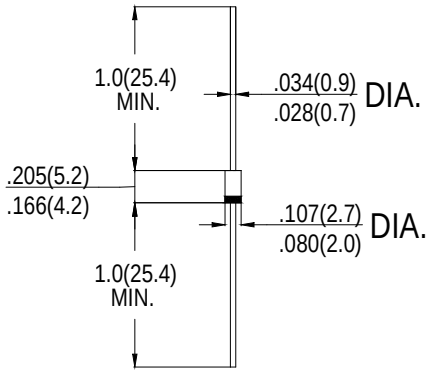

Dimensions in inches and (millimeters)

MAXIMUM RATINGS AND ELECTRONICAL CHARACTERISTICS

Ratings at 25℃ ambient temperature unless otherwise specified.
Single phase, half wave, 60Hz,resistive or inductive load.
For capacitive load, derate current by 20%

	SYMBOL	UF 4001	UF 4002	UF 4003	UF 4004	UF 4005	UF 4006	UF 4007	units
Maximum Recurrent Peak Reverse Voltage	V_{RRM}	50	100	200	400	600	800	1000	V
Maximum RMS Voltage	V_{RMS}	35	70	140	280	420	560	700	V
Maximum DC Blocking Voltage	V_{DC}	50	100	200	400	600	800	1000	V
Maximum Average Forward rectified Current at T_A=50°C	I_o	1.0							A
Peak Forward Surge Current 8.3ms single half sine-wave superimposed on rate load (JEDEC method)	I_{FSM}	30							A
Maximum Instantaneous forward Voltage at 1.0A DC	V_F	1.0				1.7			V
Maximum DC Reverse Current at Rated DC Blocking Voltage T_A=25°C	I_R	5.0							μA
Maximum Full Load Reverse Current Full Cycle Average,.375"(9.5mm) lead length at T_L=75°C		100							
Maximum Reverse Recovery Time (Note 1)	t_{rr}	50							nS
Typical Junction Capacitance (Note 2)	C_J	15				12			pF

.

Notes: 1.Test Conditions: I_F=0.5A, I_R=1.0A, I_{RR}=0.25A
2.Measured at 1MHz and applied reverse voltage of 4.0 volts

SHANGHAI SUNRISE ELECTRONICS CO., LTD.

IN4148

SILICON EPITAXIAL PLANAR
SWITCHING DIODE

REVERSE VOLTAGE: 75V
FORWARD CURRENT: 150mA

TECHNICAL SPECIFICATION

FEATURES

- Small glass structure ensures high reliability
- Fast switching
- Low leakage
- High temperature soldering guaranteed:
  250°C/10S/9.5mm lead length
  at 5 lbs tension

MECHANICAL DATA

- Terminal: Plated axial leads solderable per MIL-STD 202E, method 208C
- Case: Glass,hermetically sealed
- Polarity: Color band denotes cathode
- Mounting position: Any

DO - 35

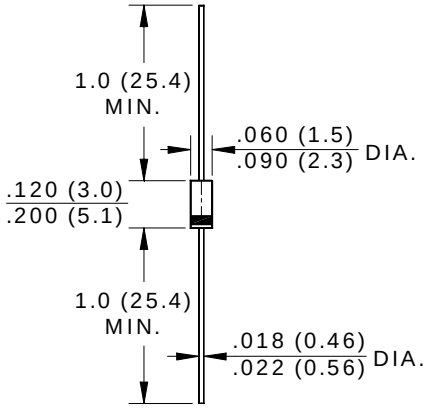

Dimensions in inches and (millimeters)

MAXIMUM RATINGS AND CHARACTERISTICS

(Ratings at 25°C ambient temperature unless otherwise specified)

RATINGS	SYMBOL	VALUE	UNITS
Reverse Voltage	V_R	75	V
Peak Reverse Voltage	V_{RM}	100	V
Forward Current (average)	I_O	150	mA
Repetitive Forward Peak Current	I_{FRM}	300	mA
Forward Voltage (I_F=10mA)	V_F	1	V
Reverse Current (V_R=20V)	I_{R1}	25	nA
Reverse Current (V_R=75V)		5	μA
Reverse Current (V_R=20V,T_J=100°C)	I_{R2}	50	μA
Capacitance (note 1)	Ct	4	pF
Reverse Recovery Time (note 2)	I_F	4	nS
Thermal Resistance (junction to ambient) (note 3)	R_θ(ja)	0.35	°C/mW
Operating Junction and Storage Temperature Range	T_{STG},T_J	-55 ～+175	°C

Notes:
1: V_R=0V, f=1 MHz
2: I_F=10mA to I_R=1mA, V_R=6V, R_L=100Ω
3: Valid provided that leads are kept at ambient temperature at a distance of 8mm from case.

http://www.sse-diode.com

ACS712

Fully Integrated, Hall Effect-Based Linear Current Sensor with 2.1 kVRMS Voltage Isolation and a Low-Resistance Current Conductor

Features and Benefits

- Low-noise analog signal path
- Device bandwidth is set via the new FILTER pin
- 5 µs output rise time in response to step input current
- 50 kHz bandwidth
- Total output error 1.5% at T_A = 25°C, and 4% at –40°C to 85°C
- Small footprint, low-profile SOIC8 package
- 1.2 mΩ internal conductor resistance
- 2.1 kV_{RMS} minimum isolation voltage from pins 1-4 to pins 5-8
- 5.0 V, single supply operation
- 66 to 185 mV/A output sensitivity
- Output voltage proportional to AC or DC currents
- Factory-trimmed for accuracy
- Extremely stable output offset voltage
- Nearly zero magnetic hysteresis
- Ratiometric output from supply voltage

Package: 8 pin SOIC (suffix LC)

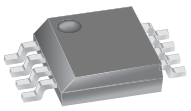

Approximate Scale 1:1 

Description

The Allegro® ACS712 provides economical and precise solutions for AC or DC current sensing in industrial, automotive, commercial, and communications systems. The device package allows for easy implementation by the customer. Typical applications include motor control, load detection and management, switched-mode power supplies, and overcurrent fault protection.

The device consists of a precise, low-offset, linear Hall sensor circuit with a copper conduction path located near the surface of the die. Applied current flowing through this copper conduction path generates a magnetic field which is sensed by the integrated Hall IC and converted into a proportional voltage. Device accuracy is optimized through the close proximity of the magnetic signal to the Hall transducer. A precise, proportional voltage is provided by the low-offset, chopper-stabilized BiCMOS Hall IC, which is programmed for accuracy after packaging.

The output of the device has a positive slope (>$V_{IOUT(Q)}$) when an increasing current flows through the primary copper conduction path (from pins 1 and 2, to pins 3 and 4), which is the path used for current sensing. The internal resistance of this conductive path is 1.2 mΩ typical, providing low power

Continued on the next page…

Typical Application

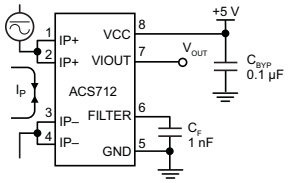

Application 1. The ACS712 outputs an analog signal, V_{OUT}, that varies linearly with the uni- or bi-directional AC or DC primary sensed current, I_P, within the range specified. C_F is recommended for noise management, with values that depend on the application.

International
IOR Rectifier

Data Sheet No. PD60046-S

IR2104(S)&(PbF)

HALF-BRIDGE DRIVER

Features

- Floating channel designed for bootstrap operation
  Fully operational to +600V
  Tolerant to negative transient voltage
  dV/dt immune
- Gate drive supply range from 10 to 20V
- Undervoltage lockout
- 3.3V, 5V and 15V input logic compatible
- Cross-conduction prevention logic
- Internally set deadtime
- High side output in phase with input
- Shut down input turns off both channels
- Matched propagation delay for both channels
- Also available LEAD-FREE

Product Summary

V_{OFFSET}	600V max.
I_O+/-	130 mA / 270 mA
V_{OUT}	10 - 20V
$t_{on/off}$ (typ.)	680 & 150 ns
Deadtime (typ.)	520 ns

Packages

8 Lead SOIC
IR2104S

8 Lead PDIP
IR2104

Description

The IR2104(S) are high voltage, high speed power MOSFET and IGBT drivers with dependent high and low side referenced output channels. Proprietary HVIC and latch immune CMOS technologies enable ruggedized monolithic construction. The logic input is compatible with standard CMOS or LSTTL output, down to 3.3V logic. The output drivers feature a high pulse current buffer stage designed for minimum driver cross-conduction. The floating channel can be used to drive an N-channel power MOSFET or IGBT in the high side configuration which operates from 10 to 600 volts.

Typical Connection

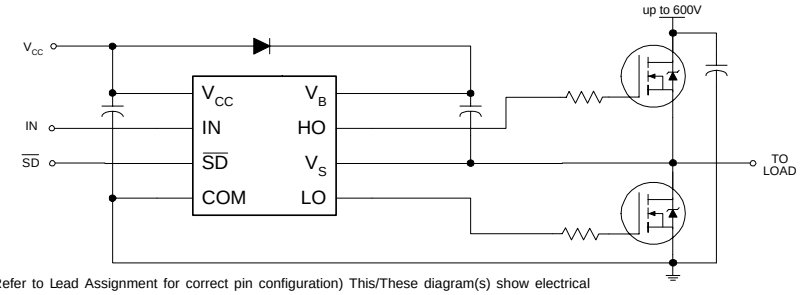

(Refer to Lead Assignment for correct pin configuration) This/These diagram(s) show electrical connections only. Please refer to our Application Notes and DesignTips for proper circuit board layout.

P6KE SERIES

GLASS PASSIVATED JUNCTION TRANSIENT VOLTAGE SUPPRESSOR

CHENG-YI ELECTRONIC

VOLTAGE 6.8 to 440 VOLTS
600 WATT PEAK POWER
5.0 WATTS STEADY STATE

DO-15

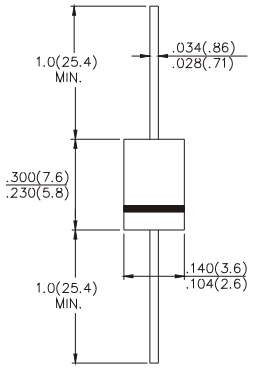

Dimensions in inches and (millimeters)

FEATURES

- Plastic package has Underwrites Laboratory Flammability Classification 94V-O
- Glass passivated chip junction in DO-15 package
- 400W surge capability at 1 ms
- Excellent clamping capability
- Low zener impedance
- Fast response time: typically less than 1.0 ps from 0 volts to BV min.
- Typical I_R less than 1 μA above 10V
- High tempreature soldering guaranteed: 260 °C/10 seconds /.375",(9.5mm) lead length/51bs.,(2.3kg) tension

MECHANICAL DATA

- Case:JEDEC DO-15 Molded plastic
- Terminals:Plated Axial leads, solderable per MIL-STD-202, Method 208
- Polarity:Color band denotes cathode except Bipolar
- Mounting Position:Any
- Weight:0.015 ounce, 0.4 gram

MAXIMUM RATINGS AND ELECTRICAL CHARACTERISTICS

Ratings at 25°C ambient temperature unless otherwise specified.
Single phase, half wave, 60Hz, resistive or inductive load.
For capacitive load, derate current by 20%.

RATINGS	SYMBOL	VALUE	UNITS
Peak Pulse Power Dissipation at T_A=25°C, T_P=1ms (NOTE 1)	P_{PK}	Minimum 6000	Watts
Steady Power Dissipation at T_L=75°C Lead Lengths .375",(9.5mm)(NOTE 2)	P_D	5.0	Watts
Peak Forward Surge Current 8.3ms Single Half Sine-Wave Superimposed on Rated Load(JEDEC Method)(NOTE 3)	I_{FSM}	100	Amps
Operating Junction and Storage Temperature Range	T_J, T_{STG}	-65 to + 175	°C

Notes: 1. Non-repetitive current pulse, per Fig.3 and derated above T_A=25°C per Fig.2
2. Measured on copper Leaf area of 1.57 in^2 (40mm^2)
3. 8.3mm single half sine-wave, duty cycle=4 pulses minutes maximum.

Transys Electronics LIMITED

IRFZ44N

Power MOSFET

V_{DSS} = 55V, $R_{DS(on)}$ = 17.5 mohm, I_D = 49 A

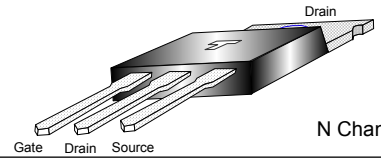

N Channel

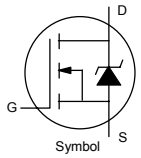

ELECTRICAL CHARACTERISICS at Tj = 25°C Maximum. Unless stated Otherwise

Parameter	Symbol	Test Conditions	Value Min	Value Typ	Value Max	Unit
Drain to Source Breakdown Voltage	$V_{(BR)DSS}$	V_{GS} = 0 V_{DC}, I_D = 250µA	55	-	-	Volt
Drain to Source Leakage Current	I_{DSS}	V_{DS} = 55V_{DC}, V_{GS} = 0V_{DC}	-	-	25	µA
		V_{DS} = 44V_{DC}, V_{GS} = 0V_{DC} Tj=150 °C	-	-	250	µA
Gate to Source Leakage Current	I_{GSS}	V_{GS} = +20V_{DC}	-	-	100	nA
		V_{GS} = -20V_{DC}	-	-	-100	nA
Gate Threshold Voltage	$V_{GS(th)}$	V_{DS} = V_{GS}, I_D = 250µA	2.0	-	4.0	Volt
Static Drain to Source On - Resistance	$R_{DS(on)}$	V_{GS}= 10V_{DC}, I_D = 10A	-	-	0.07	Ω
Gate Charge	Q_G	I_D = 25A	-	-	63	nC
Gate to Source Charge	Q_{GS}	V_{DS} = 44V_{DC},	-	-	14	nC
Gate to Drain Charge	Q_{GD}	V_{GS} = 10V_{DC}	-	-	23	nC
Input Capacitance	C_{ISS}		-	1470	-	pF
Output Capacitance	C_{OSS}	V_{DS} = 25V_{DC}, V_{GS}= 0V_{DC}, f = 1.0MHZ	-	360	-	pF
Transfer Capacitance	C_{RSS}		-	88	-	pF
Turn On Delay Time	$td_{(on)}$		-	12	-	nS
Turn Off Delay Time	$td_{(off)}$	V_{DD} = 28V_{DC}, I_D = 25A, R_G = 12Ω	-	44	-	nS
Rise Time	tr		-	60	-	nS
Fall Time	tf		-	45	-	nS
Continuous Source Current	I_S		-	-	49	A
Pulsed Source Current	I_{SM}		-	-	160	A
Forward Voltage (Diode)	V_{SD}	V_{GS} = 0V_{DC}, I_S =25A, Tp = 300µS	-	-	1.3	V
Single Pulse Avalanche Energy	E_{AS}				148	mj
Repetive Avalanche Energy	E_{AR}				9.4	mj
Avalanche Current	I_{AR}				25	A

MAXIMUM RATINGS (Tj = 25°C unless stated otherwise)

Parameter	Symbol	Condition	Value	Unit
Gate to Source Voltage	V_{GS}		+/- 20V	Volt
Drain to Source Voltage	V_{DSS}		55	Volt
Continuous Drain Current	I_D		49	Amp
Pulsed Drain Current	I_{DM}	_	160	Amp
Total Power Dissapation	P_D	(T_A = 25 C)	94	W
Thermal Resistance (Junction to Ambient)	$R_{TH\ (J-A)}$		62	°C/W

Maximum Operating Temperature Range (Tj) -55 to +175 C
Maximum Storage Temperature Range (Tstg) -55 to +175 C

Mechanical Dimensions

Case TO-220-AB Plastic

DIMENSIONS	Millimetres		Inches	
Dim	Min	Max	Min	Max
a	10.29	10.54	0.405	0.415
b	2.62	2.87	0.103	0.113
c	6.10	6.47	0.240	0.255
d	3.54	3.78	0.139	0.149
e	14.84	15.24	0.584	0.600
f	13.47	14.09	0.530	0.555
g	1.15		0.045	
h	1.15	1.400	0.045	0.055
j		2.54		0.100
k	3.550	4.06	0.140	0.160
m	4.20	4.69	0.165	0.185
n	1.22	1.32	0.048	0.052
p	2.64	2.92	0.104	0.115
q	0.48	0.55	0.018	0.022
r	0.69	0.93	0.027	0.037

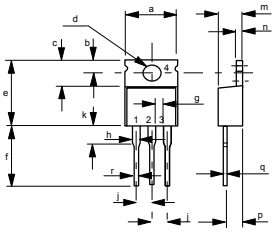

1 - Gate
2 & 4 - Drain
3 - Source

TECH PUBLIC
台舟电子

LM2596 Series

3A / 150kHz Step-Down DC-DC Converter

www.sot23.com.tw

GENERAL DESCRIPTION

The LM2596 Series are step-down switching regulator s with all required active functions. It is capable of driving 3A load with excellent line and load regulations. These devices are available in fixed output voltages of 3.3V, 5V, and an adjustable output version.

The LM2596 series operates at a switching frequency of 150kHz thus allowing smaller sized filter components than what would be needed with lower frequency switching regulators. It substantially not only reduces the area of board size but also the size of heat sink, and in some cases no heat sink is required. The ±4% tolerance on output voltage within specified input voltages and output load conditions is guaranteed. Also, the oscillator frequency accuracy is within ±10%. External shutdown is included. Featuring 100μA (typical) standby current. The output switch includes cycle-by-cycle current limiting, as well as thermal shutdown for full protection under fault conditions.

Features

- Output voltage: 3.3V, 5V & adjustable version
- Adjustable output voltage range 1.23V~38.5V
- 150kHz fixed switching frequency
- Voltage mode Non-synchronous PWM control
- Thermal shutdown and current limit protection
- ON/OFF shutdown control input
- Short circuit protect (SCP)
- Operating voltage can be up to 40V
- Output load current 3A

Applications

- Simple High-efficiency Step down Regulator
- On-Card Switching Regulators
- Positive to Negative Converter

TYPICAL APPLICATION

OUTPUT VOLTAGE	PART NO.	PACKAGE	PACKING
3.3V	LM2596SX-3.3	TO-263-5L (D^2PAK)	500pcs / 13" Reel
5.0V	LM2596SX-5.0	TO-263-5L (D^2PAK)	500pcs / 13" Reel
ADJ	LM2596SX-ADJ	TO-263-5L (D^2PAK)	500pcs / 13" Reel

Marking:

LM2596SX-3.3

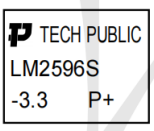

LM2596SX-5.0

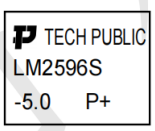

LM2596SX-ADJ

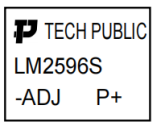

VISHAY
www.vishay.com

LCD-016N002B-CFH-ET

Vishay

16 x 2 Character LCD

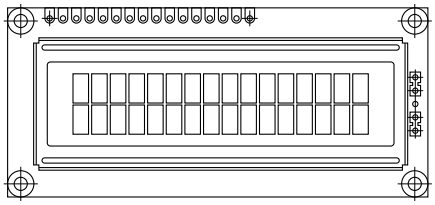

FEATURES

- Type: Character
- Display format: 16 x 2 characters
- Built-in controller: ST 7066 (or equivalent)
- Duty cycle: 1/16
- 5 x 8 dots includes cursor
- + 5 V power supply
- LED can be driven by pin 1, pin 2, or A and K
- N.V. optional for + 3 V power supply
- Optional: Smaller character size (2.95 mm x 4.35 mm)
- Material categorization: For definitions of compliance please see www.vishay.com/doc?99912

Pb-free
RoHS COMPLIANT

MECHANICAL DATA

ITEM	STANDARD VALUE	UNIT
Module Dimension	80.0 x 36.0 x 13.2 (max.)	mm
Viewing Area	66.0 x 16.0	
Dot Size	0.55 x 0.65	
Dot Pitch	0.60 x 0.70	
Mounting Hole	75.0 x 31.0	
Character Size	2.95 x 5.55	

ABSOLUTE MAXIMUM RATINGS

ITEM	SYMBOL	STANDARD VALUE			UNIT
		MIN.	TYP.	MAX.	
Power Supply	V_{DD} to V_{SS}	- 0.3	-	13	V
Input Voltage	V_I	V_{SS}	-	V_{DD}	

Note

- V_{SS} = 0 V, V_{DD} = 5.0 V

ELECTRICAL CHARACTERISTICS

ITEM	SYMBOL	CONDITION	STANDARD VALUE			UNIT
			MIN.	TYP.	MAX.	
Input Voltage	V_{DD}	V_{DD} = + 5 V	4.5	5.0	5.5	V
Supply Current	I_{DD}	V_{DD} = + 5 V	1.0	1.2	1.5	mA
Recommended LC Driving Voltage for Normal Temperature Version Module	V_{DD} to V_0	- 20 °C	-	-	5.2	V
		0 °C	-	-	-	
		25 °C	-	3.7	-	
		50 °C	-	-	-	
		70 °C	3.1	-	-	
LED Forward Voltage	V_F	25 °C	-	4.2	4.6	V
LED Forward Current - Array	I_F	25 °C	-	100	-	mA
LED Forward Current - Edge			-	20	40	
EL Power Supply Current	I_{EL}	V_{EL} = 110 V_{AC}, 400 Hz	-	-	5.0	mA

DISPLAY CHARACTER ADDRESS CODE

Display Position

	1	2	3	4	5	6	7	8	9	10	11	12	13	14	15	16
DD RAM Address	00	01	02	03	04	05	06	07	08	09	0A	0B	0C	0D	0E	0F
DD RAM Address	40	41	42	43	44	45	46	47	48	49	4A	4B	4C	4D	4E	4F